ABSTRACT

Title of Document: COMPUTATIONAL STUDIES ON THE BINDING AND DYNAMICS OF THE OSH4 PROTEIN OF YEAST AND A MODEL YEAST MEMBRANE SYSTEM

Brent Joseph Rogaski, Master of Science, 2010

Directed By: Prof. Jeffery B. Klauda
Department of Chemical and Biomolecular Engineering

Osh4 is an oxysterol binding protein homologue found in yeast that is essential for the intracellular transport of sterols. It has been proposed that Osh4 acts as a lipid transport protein, binding a single sterol residue and transporting it from the endoplasmic reticulum to the plasma membrane. The dynamics of Osh4 as well as ergosterol binding was observed using molecular dynamics simulations. Blind docking of several model lipid head group moieties was used to detect potential binding regions along the Osh4 surface favorable towards phospholipid interaction. Models frequently docked to a lysine-rich region on the side of the protein's β-barrel. A model ergosterol-containing membrane system for yeast was also constructed and simulated using molecular dynamics, and an improvement to the deuterium order parameters was observed over previous models. Understanding how Osh4 attaches to cellular membranes will lead to a clear understanding of how this protein transports sterols *in vivo*.

COMPUTATIONAL STUDIES ON THE BINDING AND DYNAMICS OF THE OSH4 PROTEIN OF YEAST AND A MODEL YEAST MEMBRANE SYSTEM

By

Brent Joseph Rogaski

Thesis submitted to the Faculty of the Graduate School of the
University of Maryland, College Park, in partial fulfillment
of the requirements for the degree of
Master of Science
2010

Advisory Committee:
Professor Jeffery Klauda, Chair
Professor Panagiotis Dimitrakopoulos
Professor Srinivasa Raghavan

Dedication

This thesis is dedicated to my mother and father. Nothing I have accomplished would have been possible without your continued loving support.

Acknowledgements

I would like to thank my advisor, Dr. Jeffery Klauda, for his invaluable guidance throughout the course of this project. I would also like to thank Dr. Klauda and Dr. Richard Pastor for investing their time in helping me as a student, and for financially assisting me along the way.

Table of Contents

*Chapters contain select material from:

Rogaski, B., Lim, J.B. & Klauda, J.B. (2010). Sterol binding and membrane lipid attachment to the Osh4 protein of yeast. *J. Phys. Chem. B* **114**, 13562-13573.

List of Figures

Atomistic representations from all simulations were constructed through use of the 'Visual Molecular Dynamics' program.[1]

List of Tables

CHAPTER 1 – BACKGROUND

1.1 Intracellular Sterol Transport

1.1.1 Sterols and their Cellular Distribution

Sterols are a subgroup of steroids that are characterized by three parts: a ring region consisting of three six-membered rings and one five-membered ring, a hydrophobic tail region extending from the five-membered ring at the C_{27} carbon, and a hydroxyl group on the C_3 ring carbon (Figure 1.1). Cholesterol, which is found in human and other mammalian cells, is highly important to both the form and function of cellular membranes. Given its rigid, flat, and hydrophobic ring structure, the concentration of cholesterol in a membrane can regulate membrane fluidic properties.[2] Furthermore, cholesterol has been implicated in many transmembrane signaling and trafficking processes.[2] Human cells are able to acquire cholesterol from two sources: dietary intake and *de novo* synthesis within the endoplasmic reticulum (ER).[2] The exact ratio of total body cholesterol synthesized versus that obtained from dietary sources varies from each individual, but is estimated to be approximately 70:30.[3]

Yeast (*Saccharomyces cerivisiae*), which is an established model organism for the study of biological sterol transport, does not uptake sterols from its environment under aerobic conditions and, instead, relies solely on sterol production through biosynthesis in the ER.[2; 4] Unlike in human and other mammalian cells, the dominant sterol in yeast and other fungi is ergosterol. While ergosterol is structurally similar to cholesterol, a few key differences exist in both the ring and tail regions (Figure 1.1). Namely, the ergosterol ring

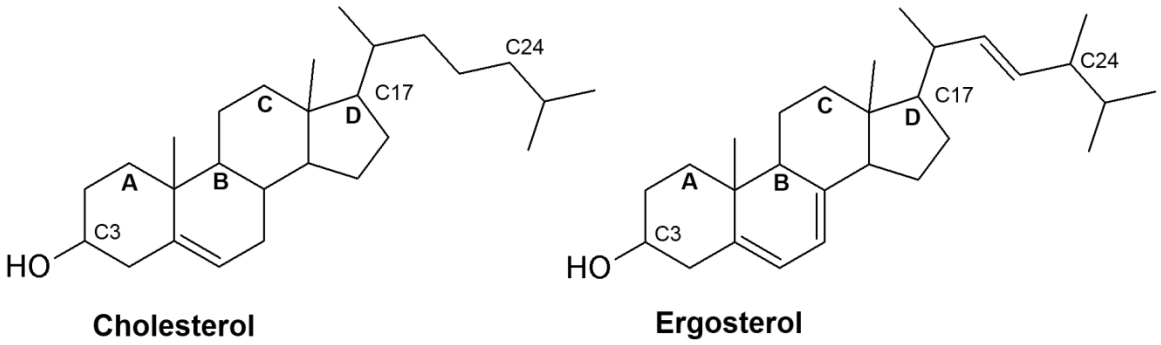

Figure 1.1 – Structures of cholesterol and ergosterol. Rings and selected carbons are labeled using the IUPAC recommended numbering scheme for a steroids.

structure is more ridged on account of an additional double bond on the B ring. The ergosterol tail is more ridged as well because of the presence of a double bond. An additional methyl group attached to the C_{24} carbon is also present on the ergosterol tail. While the differences in structure between cholesterol and ergosterol may be similar, cholesterol cannot substitute for ergosterol in yeast, as both have distinct effects on membrane properties.[5]

Sterol concentrations are not homogeneous across different organelles within the cell. The plasma membrane (PM) contains the highest sterol concentration, constituting ~35-40% of the membrane's lipid content by molecular concentration in eukaryotic cells.[6] Conversely, sterol concentration in the ER is significantly lower, constituting only ~1-10% of membrane lipid molecules.[4] Transferring sterols from the ER to the PM, as well as other membranes within the cell, would result in equilibrated sterol concentrations if it were not for a highly precise sorting mechanism.[7] The cellular processes governing the synthesis, sorting, and transport of cholesterol and other biologically important sterols are highly complex and, unfortunately, poorly understood. Mechanisms for sterol trafficking can be divided into two general classifications;

vesicular and non-vesicular mechanisms. These two mechanisms will be discussed in the following two subsections.

1.1.2 Vesicular Transport Mechanisms

One pathway for sterol transport is along the protein secretory pathway, which crosses through the Golgi.[6] Sterols are transferred to the trans-Golgi network (TGN) at a direct membrane contact site formed between the ER and the TGN.[2] In the TGN, sterols associate with sphingolipids to form lipid raft microdomains.[7] Lipid rafts are regions on the exoplasmic leaflet consisting of sphingolipids and sterols with sterols packed in between the spaces of the sphingolipid saturated chains.[8] These domains are saturated with sterols when compared to other regions on the membrane.[9] Lipid rafts are thought to exist in the liquid-ordered phase, distinct from the liquid-disordered phase in the other, more loosely packed portions of the membrane.[8] These lipid rafts are transported from the TGN to the PM through secretory vesicles (SVs), along with proteins and sterol poor domains. Vesicles are carried to the PM over cytoskeleton tracks in a manner dependent on ATP.[2] However, disruption of the cytoskeleton has shown no effect on rapid sterol transport between the ER and PM and Golgi disassembly only decreases nascent cholesterol transport by ~20% in cells.[6] Therefore, sterols are not trafficked from the ER to the PM by vesicular means alone and sterol transport along the secretory pathway appears to play only a minor role in intracellular sterol trafficking. A diagram of intracellular sterol transport pathways is shown in Figure 1.2, with the vesicular pathway displayed with red arrows.

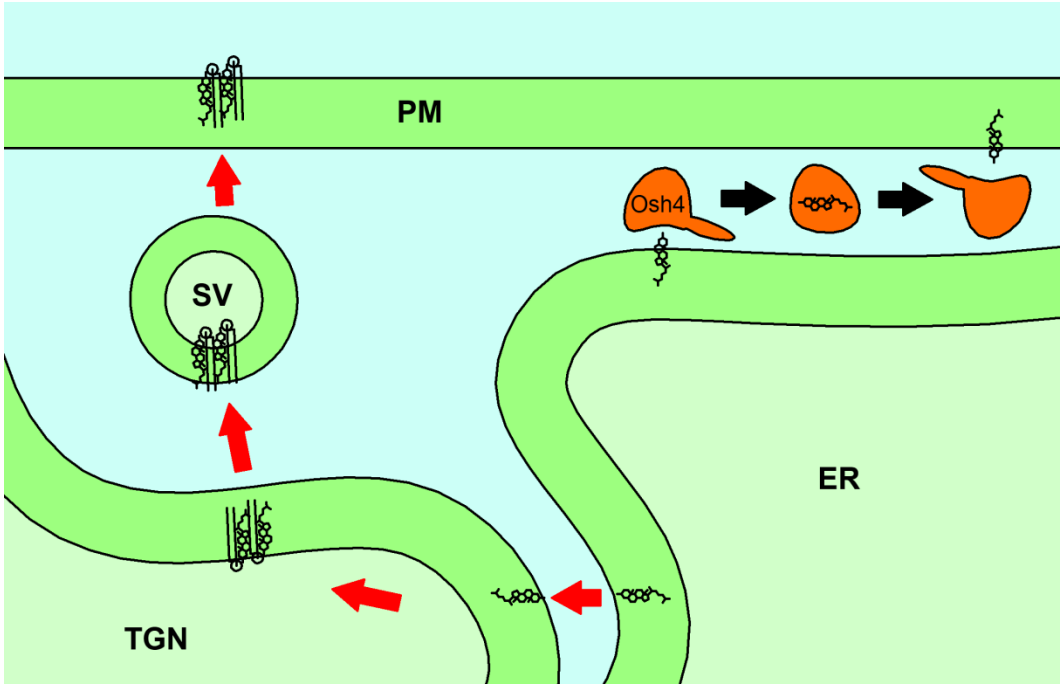

Figure 1.2 – Some proposed mechanisms of intracellular ER to PM sterol transport. The vesicular pathway is shown in red arrows, while a possible non-vesicular pathway involving Osh4 is shown with black arrows.

1.1.3 Non-vesicular Transport Mechanisms

The major pathway in which cholesterol is transferred from the ER to the PM is likely through non-vesicular mechanisms.[6] Lipid transport between membranes through lipid transport proteins (LTPs) has previously been identified for other lipids, such as the transport of ceramide via the ceramide transfer protein (CERT).[10] While the mechanisms by which proteins can extract and transfer sterols between membranes *in vivo* remains unknown, several families of proteins have demonstrated the ability to extract and transfer sterols between membranes *in vitro*. One such protein, the steroidogenic acute regulatory protein (StAR) is necessary for the efficient transport of cholesterol from the outer mitochondrial membrane to the inner mitochondrial membrane.[11] Another protein, NCP2, has shown the ability to bind with cholesterol. Mutations in either the NPC1 or

NPC2 genes are the cause of Niemann Pick Type C disease, a rare disorder that affects cholesterol storage.[11] The oxysterol-binding protein (OSBP) and its related proteins (ORPs) form a family of LTPs in humans and other mammals are grouped together based on the presence of an OSBP-related domain (ORD).[11] There are at least twelve ORPs encoded in mammals.[7] While the function of many of these proteins remains unknown, many are thought to affect processes such as lipid distribution, lipid metabolism, and vesicular trafficking.[7]

Yeast contains seven ORPs, known collectively as Osh (OSBP-homolog) proteins.[11] Unlike mammals, yeast does not posses StAR or NPC2 proteins, suggesting that the Osh proteins are responsible for non-vesicular sterol regulation and transfer (Figure 1.2, black arrows).[12] The deletion of all seven Osh genes results in death, but the organism remains viable, though with impaired function, if only one Osh gene is present suggesting an overlapping function between all Osh proteins.[13] The most abundant Osh protein, Osh4, has been shown to transfer sterols between donor and acceptor vesicles *in vitro*, with transfer stimulated in the presence of phospoinosides (PIPs).[14] Background information specific to the Osh4 protein is presented in Section 2.1.

1.2 Computational Techniques

While computational techniques have been employed in biological research for decades, the recent explosion in new technology and faster computer hardware has greatly expanded the boundaries of what researchers are capable of achieving *in silico*. While there are many applications for computer aided modeling within the realm of biochemistry and molecular biology, two techniques are presented within this subsection: Molecular dynamics (MD) simulation and docking. MD is often used to view the

dynamical properties of biomolecules while also providing thermal averages of relevant molecular properties through use of the ergodic hypothesis.[15] However, given the large computational expense attributed to long range interactions in systems with tens of thousands or more components, MD is inherently slow. Docking, which is often used in the virtual screening of pharmaceutical compounds as well as binding site identification along a protein surface, is much quicker than MD but is more limited in application. The underlying theories behind each technique are presented below.

1.2.1 Molecular Dynamics

MD is a computational simulation technique that is a useful tool in understanding small-scale biological and other systems in atomistic detail. In MD, atomistic trajectories are constructed based on Newton's laws of motion.[16] That is, an atom with mass m that is subject to a force $\boldsymbol{F}_i$ will move based on the relationship:

$$\frac{d^2\boldsymbol{x}_i}{dt^2} = \frac{\boldsymbol{F}_i}{m} \tag{1.1}$$

with the force and position ($\boldsymbol{x}_i$) in the i=x,y,z directions. Thus, through a Taylor series expansion, the positions of any atom in this system can be calculated between any time t and any time $t_0+\Delta t$ by knowing the forces acting on the atom as well as the initial position and velocity of the atom at time t_0. By repeating this procedure, a trajectory can be formed that displays the positions of all atoms in a system over some course of time. Of course, this approach requires the initial positions and velocities of all atoms in the system to be known. Positional data is typically acquired from experimental data (for example, the x-ray crystallographic coordinates of the Osh4 protein simulated in Section 2.3) or from a theoretical model (for example, the construction of the yeast membrane system discussed in Section 3.2). Initial velocities must be assigned, and are typically

done so by applying a random number generator to the Maxwell-Boltzmann distribution at the temperature of interest.[16]

Forces or energies are calculated through evaluation of a potential energy function, termed a 'force field' which consists of bonded and non-bonded interaction parameters. The form of the CHARMM force field[17] is shown in Equation 1.2:

$$U(\vec{R}) = \sum_{bonds} K_b(b - b_0)^2 + \sum_{angles} K_\theta(\theta - \theta_0)^2 + \sum_{Urey-Bradley} K_{UB}(S - S_0)^2 + \sum_{dihedrals} K_\varphi(1 + \cos(n\varphi - \delta)) + \sum_{impropers} K_\omega(\omega - \omega_0)^2 + \sum_{\substack{non-bonded \\ pairs}} \left\{ \varepsilon_{ij}^{min} \left[\left(\frac{R_{ij}^{min}}{r_{ij}} \right)^{12} - 2 \left(\frac{R_{ij}^{min}}{r_{ij}} \right)^{6} \right] + \frac{q_i q_j}{4\pi\varepsilon r_{ij}} \right\} + \sum_{residues} U_{CMAP}(\varphi, \psi) \quad (1.2)$$

Internal terms (bond length (b), valence angle (θ), dihedral angle (ϕ), improper dihedral angle (ω), and Urey-Bradley (S)) are approximated as harmonic, with the exception of the dihedral. The terms b_0, θ_0, and ω_0 refer to the equilibrium bond length, angle, and dihedral angle respectively. S_0 is the Urey-Bradley equilibrium term and n and δ refer to the multiplicity and phase in the dihedral and φ represents the dihedral angle. Non-bonded terms account for Lennard-Jones interactions and electrostatic interactions. The terms ε^{min} and R^{min} represent the well depth and radius of the Lennard-Jones term with r_{ij} representing the distance between atoms i and j. The term q_i and q_j represent the partial charges on atoms i and j. The term ε is the effective dielectric constant. K_b, K_θ, K_{UB}, K_φ, and K_ω are constants. The CMAP correction is a 2D-energy correction term for the dihedral, and provides a better description for the protein's backbone.[17]

1.2.2 Docking

Docking techniques are generally used to predict the structure of a complex formed when a ligand molecule binds to a receptor. Thus, it is imperative to sample a wide range of possible conformations in rapid succession. These techniques have also been used to identify potential binding sites along a protein's surface when the binding location of a ligand is unknown.[18] Docking is achieved by rotating and translating a ligand about the receptor. While the receptor conformation is typically held rigid, the ligand is often set to have rotatable bonds in order to increase the conformational sampling space. While flexibility of protein side chains can be achieved in many docking suites, the added degrees of freedom dramatically increase computational time.

Conformations that are produced during docking tests are evaluated against a scoring function in order to compare how well the predicted complex performs against other predicted complexes. A search algorithm, such as simulated annealing[19] or a genetic algorithm[20], uses information produced by the scoring function evaluation to generate a new set of conformations to test. There are many docking programs available, and each has a unique scoring function. The AutoDock4 scoring function,[21] which was used for these tests, uses a free energy approach that compares the energy of the ligand and receptor separated with the energy of the ligand and receptor in complex (Equation 1.3)[21]:

$$\Delta G = (U_{bound}^{L-L} - U_{unbound}^{L-L}) + (U_{bound}^{P-P} - U_{unbound}^{P-P}) + \left(U_{bound}^{P-L} - U_{unbound}^{P-L} + \Delta S_{conf}\right) \quad (1.3)$$

The entropic term (S_{conf}) in Equation 1.3 is estimated by multiplying the torsional degrees of freedom in the ligand by an empirically derived constant. The energy (U) contains a Lennard-Jones term, an electrostatics term, a hydrogen bonding term, and a desolvation

term based on the atomic solvation parameter (ASP) implicit solvation model (Equation 1.4). Each term contains an empirically derived weighting value.

$$U = W_{LJ}\sum_{i,j}\left(\frac{A_{ij}}{r_{ij}^{12}} - \frac{B_{ij}}{r_{ij}^{6}}\right) + W_{hbond}\sum_{i,j}E(t)\left(\frac{C_{ij}}{r_{ij}^{12}} - \frac{D_{ij}}{r_{ij}^{10}}\right) + W_{elec}\sum_{i,j}\frac{q_i q_j}{\varepsilon(r_{ij})r_{ij}}$$
$$+ W_{sol}\sum_{i,j}\left(S_i V_j + S_j V_i\right)e^{\left(-r_{ij}^2/2\sigma^2\right)} \qquad (1.4)$$

The terms A_{ij} and B_{ij} are Lennard-Jones parameters taken from the AMBER[22] forcefield. The terms C_{ij} and D_{ij} are designed to assign the proper maximum well depth for atoms undergoing hydrogen bonds with directionality $E(t)$ where t is the hydrogen bond angle with respect to the ideal hydrogen bonding angle. In the desolvation term, S represents the solvation parameter and V is the estimated volume of desolvation. The term σ is an exponential weighting factor, and W_{LJ}, W_{hbond}, W_{elec}, and W_{sol} are empirically derived weighting constants.

CHAPTER 2 – LIGAND BINDING OF THE OSH4 PROTEIN

2.1 Introduction

Of the seven Osh proteins encoded within the yeast genome, Osh4 is the most highly expressed with an abundance of approximately 32,000 macromolecules per cell.[10] As of now, Osh4 is the only ORP whose crystal structure has been solved, with structures available for the protein complexed with cholesterol, ergosterol, and three hydroxycholesterols.[23] Three crystal structures of an engineered 'lidless' variant are also available where the protein exists in an unliganded state with residues 1-29 removed and the 236-240 surface loop replaced by an ectopic dipeptide sequence. Because MD and docking techniques require an initial coordinate set, Osh4 can be used with these techniques. For the liganded structures, sterols bind inside of a tunnel formed by a 19 strand β-sheet that nearly forms a complete β-barrel (Figure 2.1). A flexible N-terminal lid domain occludes the bound sterol from the aqueous phase. Recently, it has been suggested that

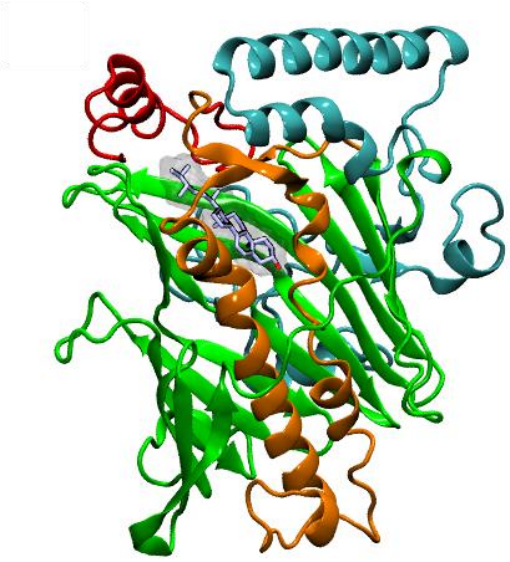

Figure 2.1 – The structure of the Osh4 protein complexed with ergosterol and divided by sub-domain . Protein regions are color coded as follows: lid region (residues 1-29) – red; central helices region (30-116) – orange; β-barrel region (117-307) – green; C-terminal region (308-434) – cyan.

the N-terminal lid forms an ArfGAP1 lipid packing sensor (ALPS) motif, a membrane binding motif that preferentially targets membranes with a high positive curvature (38 versus 90 nm liposomes).[24] This lid is thought to bind to membranes in the sterol free (*apo*) or open state, allowing for sterol uptake from the membrane.

While the ALPS motif is not found on most ORPs, several ORPs contain other functional domains located in the N-terminus with respect to the ORD. For example, the Osh1-3 proteins as well as human OSBP and several other human ORPs contain a Plecstrin homology (PH) domain.[25] Many, though not all, PH domains can bind PIPs with varying degrees of affinity.[26] Though Osh4 lacks a PH domain, its ORD is capable of binding to PIPs.[27] Furthermore, the presence of phosphatidylinositol(4,5)biphosphate (PIP_2) has been shown to stimulate cholesterol transfer between donor and acceptor liposomes *in vitro*, and may possibly serve as means for the regulation of sterol distribution between cellular compartments by ORPs.[14] Though the mechanism of interaction between PIPs and Osh4 remains unclear, it is thought that PIP binding occurs on regions of the external surface of the protein. A triple glutamate (R236E/K242E/K243E) Osh4 variant is incapable of binding to PIPs, while alterations to charged residues near the mouth of the sterol-binding pocket do not affect PIPs' ability to stimulate sterol transfer between membranes, suggesting that the flexible 236-244 surface loop may be important with regards to Osh4's ability to attach to PIP membranes.[27] However, due to the location of this loop away from the mouth of the Osh4 binding pocket, it is unclear how PIP binding to this region would help facilitate sterol extraction and delivery.

Previously, MD simulation has been used to investigate the Osh4 protein complexed with cholesterol in both Singh et al.[28] and Canagarajah et al.[29] In Singh et al., water-mediated interactions between the ring hydroxyl group of cholesterol and polar residues in the Osh4 binding pocket were found to be significant for sterol binding, while the lid had a negligible effect on stabilizing the bound sterol within the binding pocket. Additionally, a mechanism for sterol release and uptake from the cytoplasm was derived and conceptualized as a *dual molecular ladder*.[28] Stepwise cholesterol unbinding was also observed in Canagarajah et al.[29] where the rate limiting step in sterol exchange was identified as the lid opening event. In Canagarajah et al., the Osh4 α_7 helix was suggested to exist in a mobile, meta-stable state while the lid was closed and suggested to exist in a lower mobility, stable state in the *apo* conformation.[29]

The studies presented within this chapter aim to further investigate the energetics of sterol binding through MD simulations of the Osh4 protein complexed with yeast's natural sterol, ergosterol. Region specific backbone structural changes of the Osh4 protein are also examined over the course of these simulations in order to identify conformations not observable in the crystal structure. In addition, docking studies are used to probe the protein surface for regions that have affinity towards certain phospholipids that are either commonly found in yeast membranes or stimulate Osh4 mediated sterol transfer *in vitro*: phosphatidylcholine (PC), phosphatidylserine (PS), phosphatidylinositol(4,5)biphosphate (PIP_2), and phosphatidylinositol(3,4,5)triphosphate (PIP_3). The goal of this work is to better understand how the Osh4 protein binds to sterols. The docking studies with model lipid head groups will be useful for identifying potential membrane lipid attachment sites. This will, in turn, provide a better

understanding of how this protein, as well as similar human proteins with high sequential homology, attach to cellular membranes. This knowledge will be useful in ultimately understanding the mechanism to which this protein, and similar proteins, transfer biological sterols between intracellular membranes.

2.2 MD Simulation of Ergosterol in Solvent

2.2.1 Methods

Two MD simulations were conducted: One with ergosterol solvated in water and one with ergosterol solvated in ethanol. Water (TIP3P)[30] was selected as it is the primary constituent of cytosol and ethanol was selected in order model the experimental setup for the ligand binding assay experiments presented in Im et al.[23] For both simulations, ergosterol was placed at the center of a cubic box consisting of pre-equilibrated solvent. This was followed by 100 steps of steepest descent (SD) minimization and 1,000 steps of Adopted Basis Newton-Rhapson (ABNR) minimization in order to reduce unfavorable energy contacts. Both simulations were then heated from 110.15 K to 310.15 K over a period of 100 ps in CHARMM[17] using a 1-fs timestep. This was followed by 11 ns of constant pressure, temperature, and molecular (NPT) dynamics in CHARMM, of which, the last 10 ns were used for data collection purposes. Pressure was held constant at 1.0 bar using a Langevin piston and the temperature was held constant at 310.15K using the Hoover thermostat.[31] Lennard-Jones interactions were smoothed by a switching function over the 8-12 Å range and Particle Mesh Ewald (PME)[32] was used to compute long range electrostatics. All hydrogen atoms were constrained using the SHAKE algorithm.[33] Both systems used cubic periodic boundary conditions. The CHARMM C22[34] force field was

used for both simulations. Ergosterol was parameterized using existing cholesterol parameters[35] as a reference.

The ethanol solvent was prepared by creating a cubic lattice of randomly rotated ethanol residues. This was minimized with 1,000 steps SD and 1,000 steps ABNR minimization and then heated in CHARMM for 100 ps using a 1-fs timestep up to 310.15 K. This was followed by 2 ns of NPT MD simulation in CHARMM in a manner consistent with the ergosterol-ethanol simulation described above.

The ergosterol/water simulation system consisted of one ergosterol residue and 1,780 water molecules for a total size of 5,413 atoms. The ergosterol/ethanol simulation system consisted of one ergosterol residue and 1,714 ethanol residues for a total system size of 15,499 atoms.

2.2.2 Results

The interaction energy between ergosterol and solvent was calculated for both the water and ethanol simulations using CHARMM routines (Table 2.1). Ergosterol posses a higher affinity (2.53 kcal/mol) towards ethanol than water due to a higher contribution from the van der Waals (vdW) interactions between the nonpolar alkane portion of ethanol with the hydrophobic portion of ergosterol. The total interaction energy is further used in section 2.3.2 as an estimation of the solvation energy of ergosterol (ΔE^{sol}).

Solvent	Total (kcal/mol)	vdW (kcal/mol)	Electrostatics (kcal/mol)
Water	-45.34 ± 0.37	-22.39 ± 6.54	-7.86 ± 3.73
Ethanol	-47.87 ± 0.76	-29.40 ± 7.48	-4.50 ± 3.37

Table 2.1 – Interaction energy between ergosterol and solvent. The total interaction energy, as well as the vdW and electrostatic contributions to the total are shown.

2.3 MD Simulation of Osh4 in Solvent

2.3.1 Methods

A total of five MD simulations were completed on the Osh4 protein complexed with ergosterol using both the CHARMM[17] and NAMD[36] packages. The initial x-ray crystallographic structure for this protein (PDB code 1ZHZ) as well as the residue numbering scheme is taken from Im et al.[23] All waters contained in the crystal structure, as well as the liganded ergosterol residue, are maintained while the two Pb^{2+} ions were deleted. The third residue found in the crystal structure (P1) is referred to here as the first residue even though the initial crystal structure taken from the PDB contains two additional residues (M-1 and D0). These residues are not present *in vivo*. Appropriate CHARMM patches were applied to the N-terminal and C-terminal residues. The CHARMM C22 force field with CMAP correction[34; 37] was used for these simulations, with ergosterol parameters and partial atomic charges conserved from the MD simulations of ergosterol in solvent.

The protein was initially solvated in a pre-equilibrated TIP3P[30] water box using CHARMM, forming a 100×100×100 Å cubic unit cell. Minimization was conducted in CHARMM using 100 steps of SD minimization followed by 1,000 steps of ABNR minimization in order to reduce unfavorable energy contacts. The initial -10 charge on the protein was neutralized in CHARMM using a 0.15 M NaCl solution. This was followed by an additional 100 steps of SD and 100 steps of ABNR minimization. The system was heated in CHARMM from 110.15 K to 310.15 K over a period of 100 ps using a 1-fs integrator time step. The final temperature, 310.15 K, was selected for easy comparison with the Osh4-cholesterol simulations presented in Singh et al.[28] From this

initial starting point, five production runs were conducted in NAMD by varying the initial velocity seeds. Each production run was allowed to thermally equilibrate for a period of 500 ps using a 2-fs integrator time step. During this equilibration period, pressure was held constant at 1.0 bar using a Langevin piston and the temperature was rescaled ever 500 timesteps. Following equilibration, 25 ns of constant pressure, temperature, and molecular (NPT) simulation was completed. Pressure was maintained at 1.0 bar using a Langevin piston and the temperature was maintained at 310.15 K using Langevin dynamics. Lennard-Jones interactions were smoothed by a switching function over the 10-12 Å range and PME[32] was used to compute long range electrostatic potentials. Periodic boundary conditions were used and all hydrogen atoms were constrained using the SHAKE algorithm[33] in CHARMM or the RATTLE algorithm[38] in NAMD.

The solvated Osh4 system consisted of 1 protein, 1 ergosterol residue, 34 chlorine ions, 44 sodium ions, and 29,715 water molecules for a total system size 96,419 atoms. A combined total of 0.25 μs was sampled across all production runs.

2.3.2 Results

The structure of the Osh4 protein did not deviate dramatically during the course of any of the 25-ns simulations, as indicated by the root mean square displacement (RMSD) of the Osh4 C-C_α backbone atoms with respect to the x-ray crystallographic structure. Of the five production runs conducted, all RMSD values fell within the range of 1.00-3.29 Å with an average RMSD of 2.09±0.26 Å over the final 10 ns of simulation (Figure 2.2). These RMSD values indicate that Osh4 is structurally stable throughout the course of all simulations.

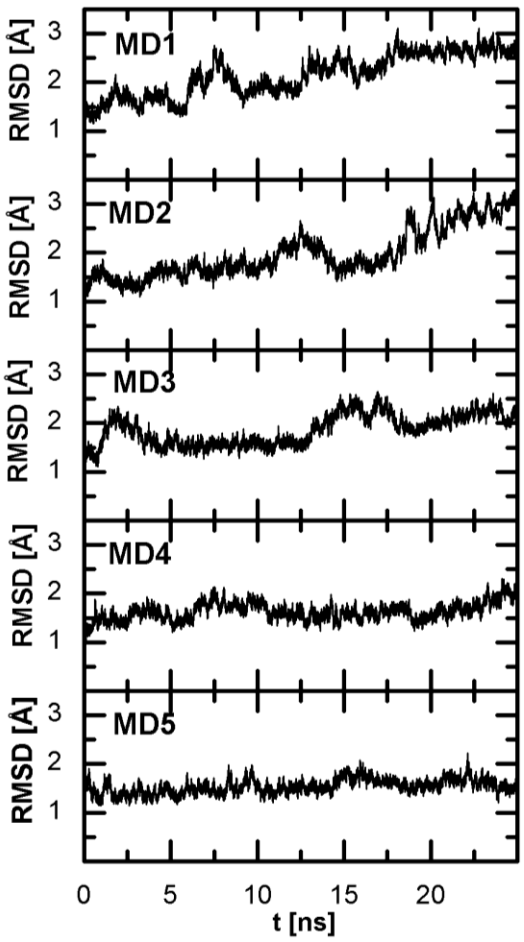

Figure 2.2 – RMSD vs. time for five Osh4/ergosterol MD simulations. All trajectories are shown separately.

Lid			Last 10 ns of simulation	
Run	Min	Max	Avg	Std
1	0.41	6.87	5.43	0.81
2	0.71	4.07	1.66	0.09
3	0.82	3.95	2.33	0.50
4	0.51	3.34	1.92	0.34
5	1.06	3.15	1.92	0.22
Central Helices			Last 10 ns of simulation	
Run	Min	Max	Avg	Std
1	0.62	1.54	1.11	0.05
2	0.69	1.65	1.15	0.06
3	0.71	1.64	1.13	0.09
4	0.72	1.54	1.06	0.09
5	0.72	1.53	1.13	0.08
Beta Barrel			Last 10 ns of simulation	
Run	Min	Max	Avg	Std
1	0.92	1.70	1.23	0.09
2	0.86	1.63	1.30	0.07
3	0.82	2.47	2.09	0.07
4	0.82	1.84	1.48	0.10
5	0.80	1.94	1.52	0.15
C-terminus			Last 10 ns of simulation	
Run	Min	Max	Avg	Std
1	0.92	3.28	1.79	0.29
2	0.72	5.36	3.50	1.07
3	0.76	3.47	1.96	0.47
4	0.84	2.59	1.50	0.27
5	0.71	3.06	1.50	0.34

Table 2.2 – RMSD of the Osh4 protein for all production runs. Minimum and maximum values are calculated from the full 25-ns trajectories while averages (Avg) and standard errors (Std) are calculated from the final 10 ns of each

In order to determine which regions of the protein contributed most to any structural deviations from the x-ray crystal structure, the RMSD of carbon backbone atoms in each sub-domain was also investigated. Sub-domains were divided in the same manner as in Im et al.[23] and are displayed in Figure 2.1. For all simulations, the structure of the β-barrel sub-domain does not deviate substantially from the x-ray crystal structure (Table 2.2). The lid sub-domain typically showed the widest range of RMSD values for all simulations. Particularly high RMSD values were observed during one trajectory, MD1 (Table 2.2), where the lid RMSD drastically increased after approximately 12 ns and eventually reaching a plateau of ~6 Å during the last 5 ns of simulation (Figure 2.3). Though the orientation of the α_1 helix (residues 9-21) remained stable during the course of these simulations, the first 6 residues or the N-terminus were found to be flexible and are responsible for the wide variation of RMSD values observed for the lid sub-domain. The flexibility of these residues has also been observed in an MD study of the Osh4 protein complexed with cholesterol by Singh et al.[28] The C-terminal sub-domain also showed a wide variability in RMSD when compared with the central helices and β-barrel sub-domains. Conformational changes on a large, surface loop consisting of residues 367-381 between the β_{18} sheet and the α_8 helix largely account for

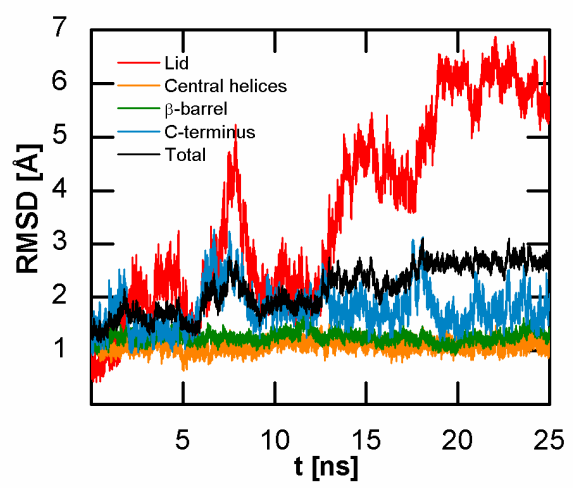

Figure 2.3 – RMSD vs. time for the MD1 simulation run of Osh4 complexed with ergosterol. Sub-domains are shown in Figure 2.1.

the observed variability in RMSD for this region. A range of RMSD values between 0.30 and 4.30 Å was encountered within this loop region. Binning of RMSD data indicates that this loop can exist in a multitude of conformations, even across the short timescales presented by this study (Figure 2.4).

The RMSD of a surface loop consisting of residues 236-244 was also investigated as this loop is thought to be potentially important with regards to membrane attachment.[27; 39] This loop was found in multiple conformations throughout the course of these simulations. Most conformational changes in this loop occurred on the order of picoseconds and were usually characterized by an RMSD change in the loop of ~1 Å followed by a several nanosecond plateau at a new value, though several intermediate conformations existed that lasted on the order of tens to hundreds of picoseconds (Figure

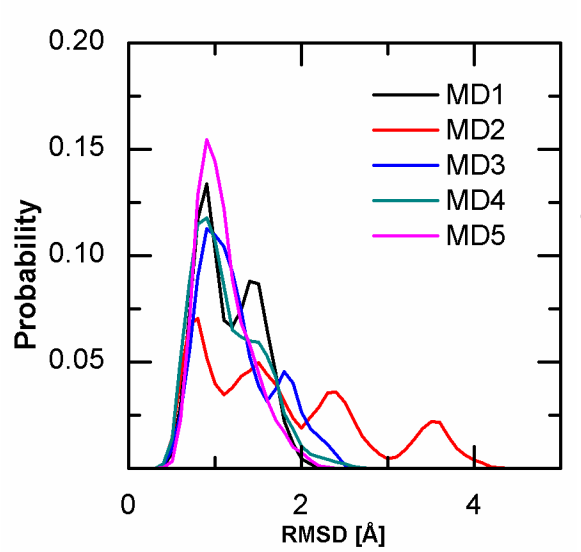

Figure 2.4 – Conformational probability of the 367-381 loop. RMSD data is binned by 0.1 Å and is collected over the entire course of all 25-ns simulations.

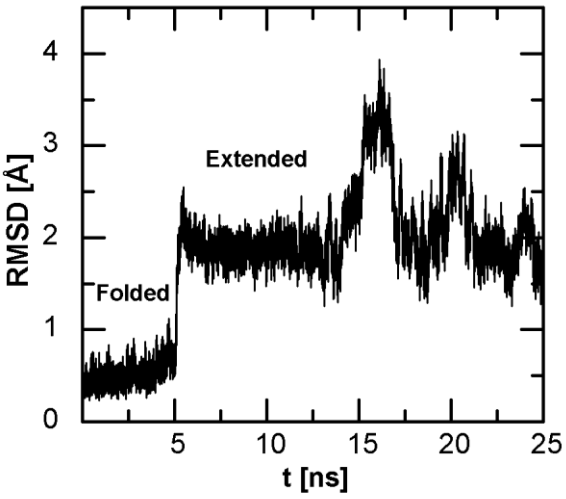

Figure 2.5 – RMSD vs. time for the 236-244 surface loop taken from the MD3 simulation run. Snapshots of this loop from this trajectory is shown in Figure 2.6.

2.5). Generally, two stable conformations for this loop were encountered: a folded conformation where the loop is folded upon itself and an extended conformation (Figure 2.6). The folded conformation was present in the proteins crystal structure. Several hydrogen bonds stabilize this conformation, including S234-S240, S245-S240, and G235-G241 backbone hydrogen bonds. A backbone hydrogen bond between Y238 and G241 was also found in this conformation, though was not as commonly encountered as the other hydrogen bonds. A hydrogen bond between the R236 side chain and the G241 backbone was also encountered. In the extended conformation, most of the stabilizing hydrogen bonds found in the folded conformation are broken. The Y238-G241 backbone hydrogen bond remains present and is more frequently encountered, and an S245-K242

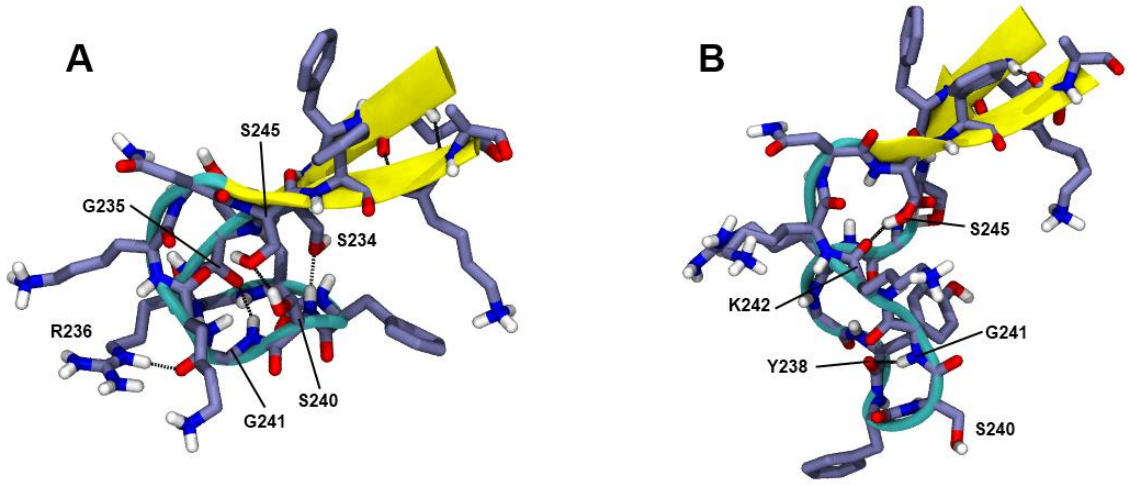

Figure 2.6 – Two stable conformations of the 236-244 surface loop. **A,** The backbone atoms of the loop are kinked so the tip runs parallel to the Osh4 surface (folded conformation). Backbone hydrogen bonds between S234-S240, S245-S240 and G235-G241 are shown. Y238-G241 backbone hydrogen bonds are found in this conformation, but are not shown. **B,** The backbone atoms of the loop adopt a more extended conformation that is more perpendicular to the Osh4 surface (extended conformation). Backbone hydrogen bonds between S245-K242 and Y238-G241 are shown. All hydrogen atoms were included in each simulation, though some are not displayed here.

backbone hydrogen bond is formed. Larger RMSD values for this region agree with the elevated mobility observed in MD simulations of Osh4 complexed with cholesterol in Canagarajah et al.[29] and agree with higher than average B-factors found in this region of the crystal structure.

The binding energies (ΔE^{bind}) of ergosterol was calculated using CHARMM routines for each simulation and then averaged. The ΔE^{bind} of ergosterol was found to be -61.10±1.26 kcal/mol, with vdW interactions contributing greater than electrostatics to the total binding energy. 83% of the total ΔE^{bind} was attributed to vdW interactions. The average binding energy relative to the solvation energy ($\Delta E^{\text{bind/sol}}$) for ergosterol was also calculated in a manner consistent with Singh et al. (Equation 2.1):[28]

$$\langle \Delta\Delta E^{\text{bind/sol}} \rangle = \langle \Delta E^{\text{bind}} \rangle - \langle \Delta E^{\text{sol}} \rangle \qquad (2.1)$$

The solvation energies of ergosterol in water and ethanol ($\Delta E^{\text{sol-wat}}$ and $\Delta E^{\text{sol-eth}}$, respectively) are reported in Table 2.1. From Equation 3.1, $\Delta\Delta E^{\text{bind/sol-wat}}$ is found to be -15.75 kcal/mol while $\Delta\Delta E^{\text{bind/sol-eth}}$ is found to be -13.23 kcal/mol. It is important to note that these binding energy calculations ignore any entropic contributions to the free energy, and rather provide an estimation of the enthalpic term. However, based on these energy calculations, it can be seen that Osh4's affinity towards ergosterol is similar in both a physiological water environment and the ethanol environment used for the binding affinity experiments presented in Im et al.[23]

Residue specific ergosterol-protein interaction energies were calculated using CHARMM routines and are shown in Table 2.3, where they are compared with the interaction energy data presented for cholesterol complexed to Osh4 taken from Singh et al.[28] Comparisons with the Osh4 protein complexed to 25-hydroxycholesterol are

Nonpolar residues	Ergosterol	Cholesterol
F13	-0.7 +/- 0.1	*-0.9 +/- 0.7*
L24	-1.2 +/- 0.2	-2.2 +/- 0.4
L27	-0.4 +/- 0.2	-0.7 +/- 0.2
I33	-1.2 +/- 0.1	-1.0 +/- 0.1
L39	-1.9 +/- 0.1	-2.0 +/- 0.2
F42	-4.0 +/- 0.2	-4.1 +/- 0.3
P110	-1.9 +/- 0.1	*-2.2 +/- 0.2*
I167	-1.8 +/- 0.1	-2.4 +/- 0.1
L177	-1.4 +/- 0.3	-1.1 +/- 0.2
V179	-1.1 +/- 0.2	-1.0 +/- 0.2
L201	-1.4 +/- 0.1	-1.6 +/- 0.2
I203	-2.3 +/- 0.2	-2.6 +/- 0.3
I206	-1.1 +/- 0.2	-1.0 +/- 0.2
P211	-1.0 +/- 0.1	-0.9 +/- 0.1
V213	-0.8 +/- 0.2	-1.1 +/- 0.1
Polar residues	**Ergosterol**	**Cholesterol**
W46	-1.0 +/- 0.5	-1.1 +/- 0.5
Q96	-4.9 +/- 1.3	-4.5 +/- 0.9
Y97	-3.1 +/- 0.2	-3.9 +/- 0.3
N165	-2.1 +/- 0.3	-2.1 +/- 0.5
Q181	-2.1 +/- 0.3	-2.7 +/- 0.5
Charged residues	**Ergosterol**	**Cholesterol**
E107	-4.0 +/- 0.2	*-5.1 +/- 0.2*
K108	-2.4 +/- 0.2	*-1.1 +/- 0.2*
K109	-2.7 +/- 0.1	-2.7 +/- 0.2

Table 2.3 – Averaged interaction energies between sterols and significant nearby residues. Most cholesterol data is taken from Singh et al., where electrostatics are not included in the interaction energies for nonpolar residues. Residues in italics were provided from the authors of Singh et al., and do include electrostatics for nonpolar residues.

presented in Rogaski et al.[40] Nonpolar residues in the Osh4 binding tunnel showed similar interaction energies when compared with those of cholesterol for most cases. However, some anomalies existed due to the structural differences between ergosterol and cholesterol (Chapter 1, Figure 1.1). Interactions between the cholesterol and ergosterol tails with charged residues near the mouth of the binding pocket (E107 and K108) varied significantly. Backbone atoms in K108 and K109 form vdW interactions on one side of each sterol's tail while hydrophobic residues (L241, L177, and I203) form vdW interactions with the other side of the tail. The E107 side chain is positioned near the five membered sterol ring, and also displayed significant variation in terms of interaction with ergosterol versus interaction with cholesterol. As the positioning of the ergosterol tail did not change significantly during the course of MD simulation, the marked differences in interaction energy for L24, E107, and K108 when compared with

cholesterol can be explained by the differences in structure and composition of each sterol's respective tail.

Of the polar residues situated at the bottom of the binding pocket, Q96 displayed the most favorable interaction energy with ergosterol. Additionally, this residue displayed the most favorable electrostatic interaction energy contribution (-2.4 kcal/mol). For all MD simulations conducted, the block-average computed standard error of the interaction energy between Q96 and ergosterol was also significantly higher than those reported for other residues. Interaction energy data for Q96 over all five simulations was combined and binned by 0.1 kcal/mol intervals. Through binning, Q96 displayed two distinct energetic peaks separated by approximately 5 kcal/mol, which is shown in Figure 2.7. The binned Q96 interaction energy data was fitted to multiple (4) Gaussian distributions in order to estimate the total probability associated with each dominant peak. By integrating all Gaussian fits associated with each energy state, it was found that the lower energy state was encountered 21% of the time over all ergosterol simulations while the higher energy state was encountered 79% of the time over all simulations. The maximum frequency for the lower and higher energy states from the interaction energy histogram were -9.2 kcal/mol and -4.1 kcal/mol, respectively. The lower energy peak is attributed to direct hydrogen bonding between Q96 and ergosterol's hydroxyl group while the higher energy peak is attributed to non-hydrogen bonded configurations or water-mediated hydrogen bonded configurations. Samples of observed binding configurations taken from MD simulation are shown in Figure 2.8.

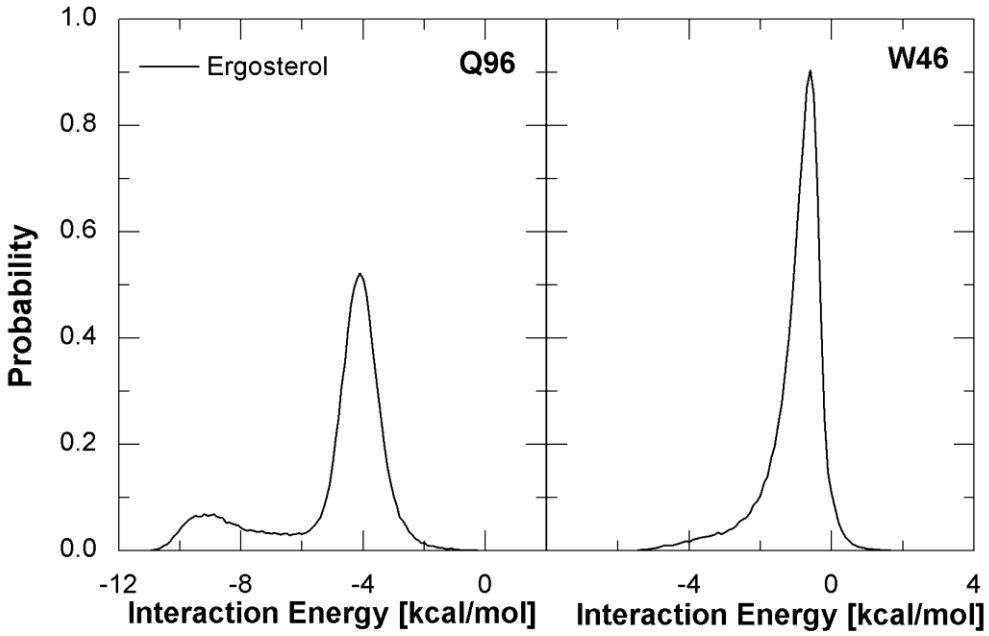

Figure 2.7 – Interaction energy probability between ergosterol and select Osh4 residues.

A similar analysis was conducted on all other residues displaying significant interaction with ergosterol, and no other residue exhibited the same two peak pattern as Q96. However, the interaction energy of W46 displayed a highly skewed distribution (Figure 2.7) that may possibly contain a small peak obscured under the tail of a much larger peak. On occasion, polar atoms on W46 did come in close enough contact with the ergosterol hydroxyl group to form direct hydrogen bonds, but generally for only a short duration. Any direct hydrogen bonding between ergosterol and W46 appears to be unstable.

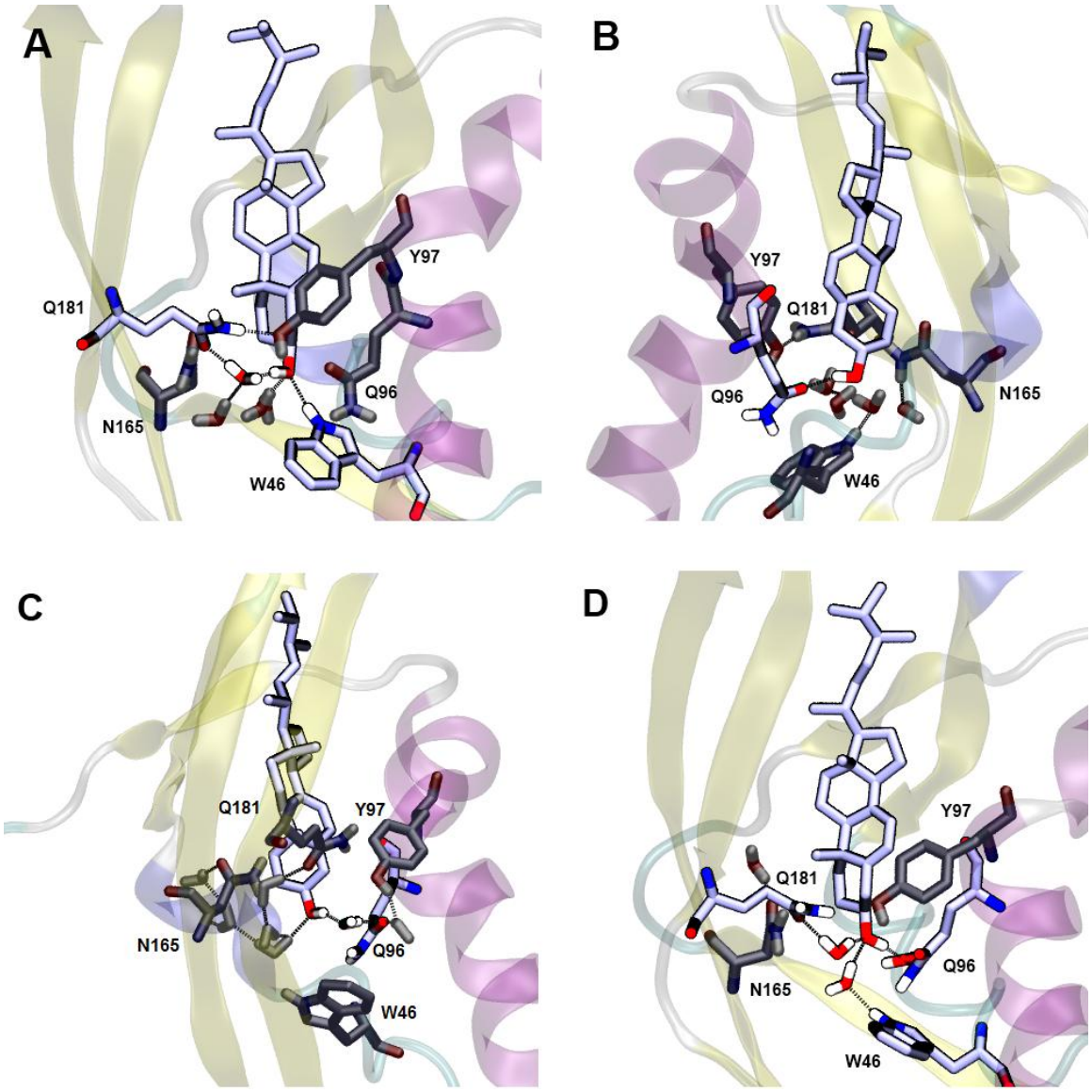

Figure 2.8 – Sample binding conformations of ergosterol with Osh4. **A,** Ergosterol forming a direct hydrogen bond with W46 as well as a water-mediated hydrogen bond with Q181. **B,** Ergosterol forming a direct hydrogen bond with Q96. **C,** Ergosterol forming a water-mediated hydrogen bond with Q96. **D,** Ergosterol forming multiple water-mediated hydrogen bonds with W46, Q96, and Q181. Nonpolar hydrogens were simulated, but are not shown. Hydrogen bonds are shown as dashed lines.

2.4 Docking of Model Lipid Head Groups to the Osh4 Surface

2.4.1 Methods

Four model head groups were chosen for blind docking against the Osh4 surface, PC, PS, PIP_2, and PIP_3. The two inositol lipids, PIP_2 and PIP_3, were chosen because their presence within a membrane has been shown to increase sterol transport between donor and acceptor vesicles *in vitro*.[14] PS was also chosen because increased PS concentration within a membrane has been correlated to an increase of sterol transfer between donor and acceptor liposomes *in vitro*, while also being enriched in the yeast plasma membrane (PM) *in vivo*.[39; 41] PC was selected because it is enriched in the yeast endoplasmic reticulum (ER) *in vivo*.[41] Model head groups were constructed by truncating existing lipid coordinate files at the C_2 carbon (Figure 2.9). Coordinates for the PC and PS models were derived from dioleoylphosphatidylcholine (DOPC) and palmitoyloleoylphasphatidylserine (POPS) coordinates taken from an MD simulation of a model yeast membrane (Chapter 3). Coordinates for PIP_2 and PIP_3 were similarly derived from their

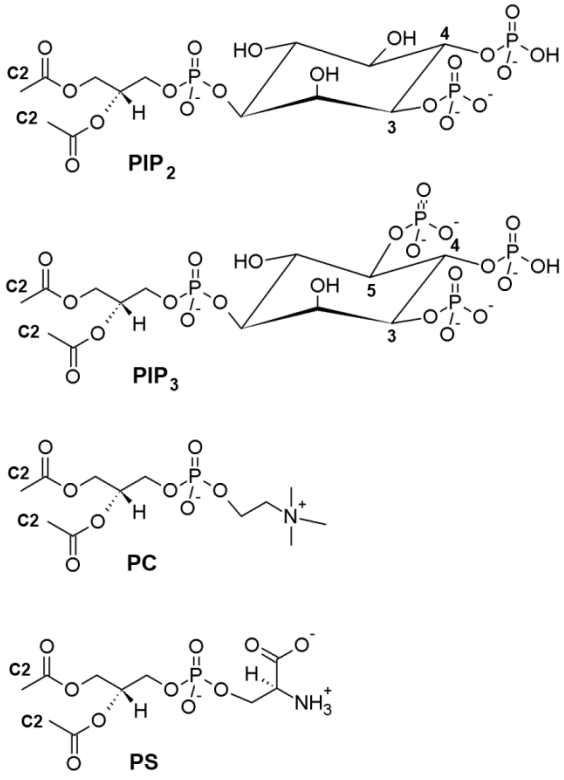

Figure 2.9 – Structures of the four model lipid compounds used for docking against the Osh4 protein surface.

corresponding structures as presented in Li et al.[42] For better sampling of protein structural conformations and side chain positioning, 5 snapshots were taken across 5-ns intervals from the MD1 and MD2 trajectories from the MD simulations of ergosterol complexed with Osh4. Two trajectories from MD simulations of Osh4 complexed with 25-hydroxycholesterol that were conducted by Joseph Lim and presented in Rogaski et al.[40] were also sampled across 5-ns intervals, as well as the crystal structure of Osh4 bound to ergosterol and the crystal structure of Osh4 bound to 25-hydroxycholesterol for a total of 22 conformational snapshots. All bound sterol moieties and solvent molecules were removed prior to docking. Additionally, each ligand was docked against the crystal structures of the engineered 'lidless' Osh4 protein taken from Im et al. (PDB code 1ZI7).[23]

Gasteiger-Marsili[43] chargers were applied to each model ligand in AutoDockTools4 (ADT4),[44] and non-integral charges were manually adjusted in order to maintain the proper charge associated with each phosphate group. Protein atomic partial charges were conserved from the MD simulations used to produce the coordinates. Ligand bonds were allowed to be freely rotatable, but receptor bonds were held rigid. All docking tests used the Lamarckian Genetic Algorithm[20] for searching and the default AutoDock4 (AD4)[44] parameter set was used. The surface of the protein was searched using a 120×120×120 point grid with a grid spacing of 0.625 Å. Each conformational snapshot was docked 25 times for twenty-five million iterations per instance for each ligand studied, producing a total of 550 results. Each engineered lidless conformation was docked 50 times, producing an additional 150 results. All docking tests were performed in AD4.

For each model compound tested, docking results for all conformations were pooled and the twenty conformations pertaining to the lowest AD4 free energy of binding (ΔG^{bind}) were selected for further analysis. These conformations are referred to as the 'top results'. Because multiple receptor conformations were sampled for each model compound, clustering results by RMSD is not an ideal way to detect different binding sites using these tests. Instead, potential binding regions are segregated based on similar interacting residues. All results from the native Osh4 structures are pooled separately from the engineered lidless results.

Docking with select flexible side chains was conducted on two regions of the protein using the PIP_2 model ligand. The first region was identified by an area of the Osh4 surface that showed the highest tendency to dock model lipids in the blind docking tests. This region was confined by a 100×100×100 point grid with a grid spacing of 0.375 Å, and was centered near the surface residue K180. As AD4 has a limit of 32 freely rotatable bonds for any given system, only select basic residues (K168, K180, K407, and K411) were set to have freely rotatable side chains. These residues had the highest tendency to interact with model ligands during the blind docking tests. The protein conformation most favorable towards PIP interaction during the blind docking tests was chosen as the receptor, and the PIP_2 model was docked to this conformation 400 times with 2.5 million iterations per instance. Docked conformations were ranked by ΔG^{bind} and the top 40 conformations were chosen as the 'top results'.

Two docked conformations from the top results were selected for MD testing to ensure the stability of the docked conformation. Coordinates from these two conformations were input into CHARMM, where hydrogens were built. Protein atoms

were then fully constrained while the PIP_2 model was subject to SD and ABNR minimization. The structure was then solvated in a 100×100×100 Å TIP3P[30] water box and neutralized with a 0.15 M NaCl solution in CHARMM. This structure was equilibrated for 100 ps in NAMD at 310.15 K using a 2-fs integrator timesetep. Temperature was rescaled every 500 timesteps, and pressure was held constant at 1.0 bar using a Langevin piston. Equilibrated structures were subject to a production run of 500 ps in NAMD in the NPT ensemble where pressure was maintained at 1.0 bar using a Langevin piston and the temperature was maintained at 310.15 K using Langevin dynamics. Lennard-Jones interactions were smoothed over the 10-12 Å range and PME[32] was used for long range electrostatics. Periodic boundary conditions were used, and hydrogens were constrained using the RATTLE algorithm.[38]

The second region analyzed by flexible residue docking was created by defining a sample space surrounding the 236-244 surface loop with a 100×122×100 point grid with a grid spacing of 0.375 Å centered about the center of the loop. All appropriate side chains (R236, Y238, F239, S240, K242, and N244) contained in the loop were set as freely rotatable bonds. Two protein conformational snapshots were used that pertained to the folded and extended conformations observed in this loop during MD simulation. PIP_2 was docked to each conformation 400 times with 2.5 million iterations per instance. Docked conformations were ranked by ΔG^{bind} and the best 40 results were selected as the 'top results'.

2.4.2 Results

Of the model lipid compounds tested, the PC model presented the greatest diversity in terms of total number of binding sites identified in the top selected results. For this model, four different binding regions (Figure 2.10) were identified when docked against the crystal and MD snapshot conformations (Table 2.4). Two of these regions were also identified during the PIP_2 tests while only one of these regions was found during the PIP_3 and PS tests (Table 2.4). All regions identified during the PS, PIP_2, and PIP_3 tests were also identified during PC blind docking tests. High negative charges associated with the PIP models (-4 for PIP_2 and -6 for PIP_3) prevented docking to PC sites where near equal distributions of positively and negatively charged amino acids were encountered. This reduced the number of docked regions identified in PIP models compared to the PC model. However, given the electroneutrality of the PC model and its small size, nearly 50% of the results had to be rejected due to docking inside of the sterol binding pocket of the Osh4 protein. The docking of model lipids to within the sterol binding pocket occurred as a result of a vacant sterol binding pocket. This issue was more prevalent in conformations taken from MD snapshots of Osh4 complexed with 25-hydroxycholesterol than in conformations taken from Osh4 complexed with ergosterol. There were no instances of either of the PIP models docking inside of the Osh4 sterol binding pocket during these tests and instances where PS docked inside of the pocket were rare.

The five trajectories from the MD simulations of Osh4 complexed with ergosterol and the five trajectories from the MD simulations of Osh4 complexed with 25-hydroxycholesterol conducted by Joseph Lim and presented in Rogaski et al.[40]

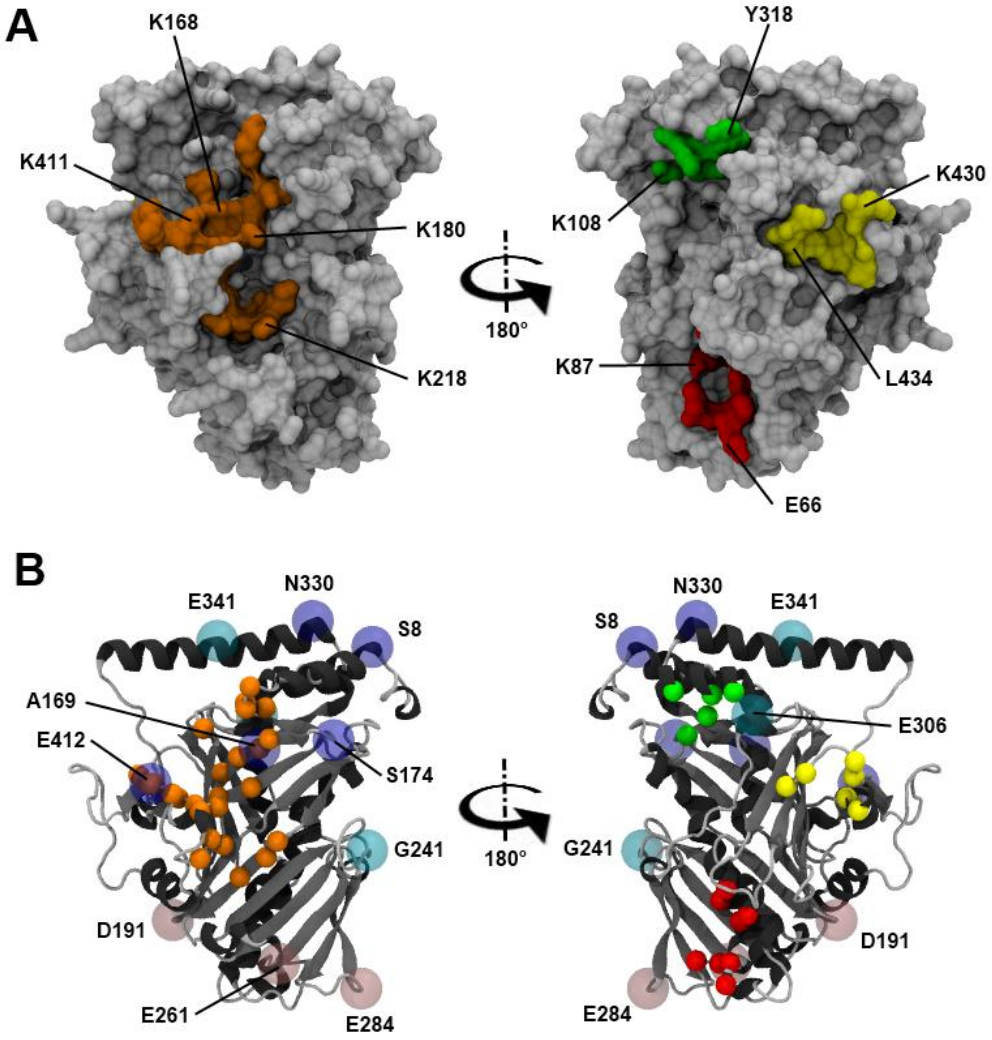

Figure 2.10 - Typical binding sites encountered by docking the PC model against the native Osh4 protein. **A,** A surface representation of the β-crease region (left) is shown in orange with select residues labeled. The opposite side of the protein is shown (right) with the α_3 region in red, the C-terminus region in yellow, and the α_4-α_6 region in green. **B,** Representation of the β-crease region (left) displaying Osh4 secondary structure with interacting residues found in the β-crease site displayed as spheres positioned at the C_α carbons. The α_3, C-terminus, and α_4-α_6 regions are shown on the opposite side of the protein. Residues found experimentally to be important to membrane binding from Schulz et al. are labeled and displayed as purple (front binding surface), pink (distal binding surface), and cyan (neither front nor distal) spheres.

Ligand	Cluster	Interacting Residues	Avg. Energy
PC	α_3	E51, E55, E66, H67, C68, L69, A84, K87	-2.94
	β-crease	D21, G22, D23, L24, P145, Q166, K168, A169 S170 , K180, F182, G217, K218, Y220, N397 A398, P399, G401, T402, L403, E408, K411 E412, D413, L414, S415	-2.47
	C-terminus	W426, D427, E429, K430, V433, L434	-2.61*
	α_4-α_6	P36, K108, Y318, A321, K325	-2.46*
PS	β-crease	G22, D23, L24, S25, H143, H144, P145, P146 Q166, I167, K168, A169, S170, T178, K180 Q181, F182, P200, G217, K218, E232, S234 G237, Y238, F239, S240, N397, P399, S400 G401, T402, L403, D406, K407, E408, K411, L414	-4.73
PIP_2	β-crease	F20, G22, P145, Q166, I167, K168, A169, S170 T178, K180, F182, P200, H202, E216, G217 K218, Y220, G237, Y238, F239, K258, A398 P399, S400, T402, D406, K407, E408, K411	-4.06
	α_4-α_6	Y45, S95, S99, R100, S103, L104, K108, K325	-4.08*
PIP_3	β-crease	F20, D23, K168, A169, S170, T172, K173, T178 K180, F182, H202, E216, G217, K218, Y220 K258, P399, S400, G401, T402, L403, D406 K407, E408, K411	-3.99

Table 2.4 - Osh4 residues found to interact with docked ligands for rigid receptor tests. Only conformations found in the top results are shown and factored into the average binding energies. Average energies denoted with an asterisk only contained one conformation in the top results.

were analyzed using the program HOLE,[45] which measures the diameter of a pore within a macromolecule along a vector that runs from the bottom of the binding pocket towards the opening created by removal of the lid residues . Because the binding pocket of Osh4 is fully enclosed, the lid residues were deleted for this analysis. The average size of the Osh4 binding pocket was nearly identical for both sterol ligands (Figure 2.11). Therefore, the increased likelihood for Osh4/25-hydroxycholesterol to accept small model compounds within the binding pocket when compared to Osh4/ergosterol is most likely caused by the side chain positioning at the instants when the snapshots were taken.

The four binding regions identified for the PC model are color-coded in Figure 2.10. Among all of the top results, the α_3 region produced the conformation exhibiting the most favorable ΔG^{bind} (-3.26 kcal/mol). However, only two out of the twenty selected results for this test were contained in this region. The α_3 region is located near the distal side of the protein, interacting with residues on the solvent exposed portion of the α_3 and α_4 helices as well as the surface loop that connects them. Both conformations in this region were stabilized through electrostatic interactions between a glutamic acid residue (E51/E59) and the choline group of PC as well as electrostatic interactions between a lysine side chain (K87) and the phosphate group of PC (Figure 2.12A). Another PC binding site (C-terminus region) was stabilized through electrostatic interactions with residue types similar to those found in the α_3 region. This region was not frequently encountered during testing, constituting only one of the top results with a ΔG^{bind} of -2.49 kcal/mol (Figure 2.12B). Similarly, the α_4-α_6 region only constituted one of the top results with a ΔG^{bind} of -2.46 kcal/mol. Of these three sites, only the α_4-α_6 region was also encountered when docking with PIP models. This region appeared during PIP_2 tests but was only found in one of the top results for this model (-4.08 kcal/mol, Figure 2.12B) and did not appear in any of the PIP_3 top results.

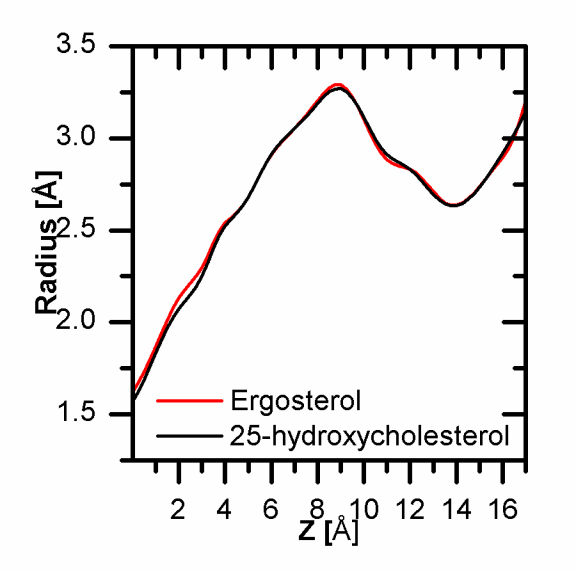

Figure 2.11 – Pore radius of the Osh4 binding tunnel complexed to two distinct sterol ligands. Averages were computed over 25-ns MD trajectories.

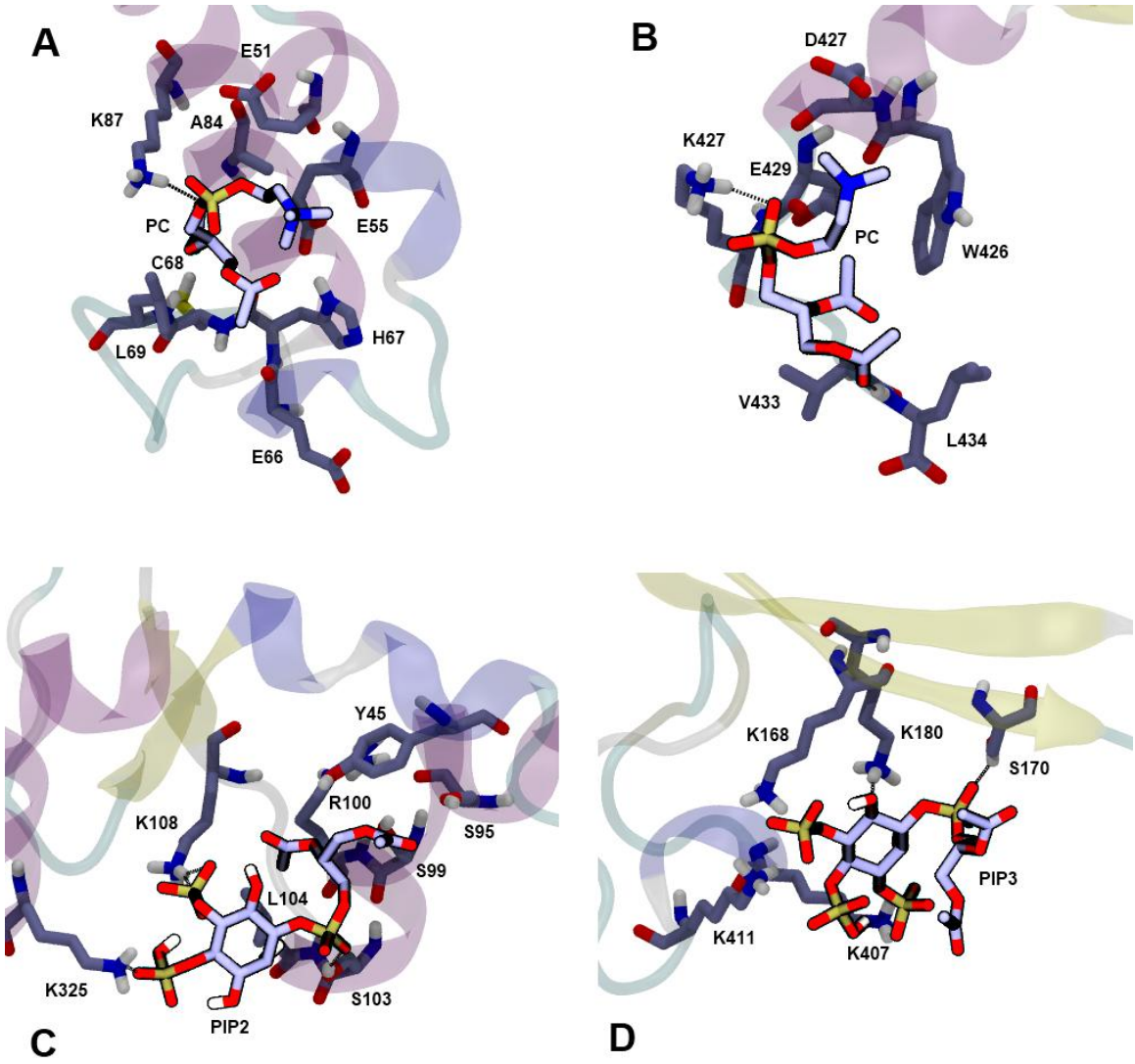

Figure 2.12 - Sample binding conformations of PC, PIP_2, and PIP_3 model ligands. **A,** A sample α_3 conformation produced through rigid-receptor docking of PC (highlighted). **B,** C-terminus region conformation produced through rigid-receptor docking of PC (highlighted). **C,** An α_6 region conformation produced through rigid-receptor docking of PIP_2 (highlighted). **D,** A sample β-crease region conformation produced through rigid-receptor docking of PIP_3 (highlighted). Osh4 residues interacting with docked ligands are displayed and labeled.

The β-crease region was located near the mouth of the sterol binding pocket, centered near K180, and was defined by a crease between a solvent accessible portion of the β-barrel and a large surface loop towards the C-terminal end of the protein. This site was the most prevalent binding site encountered during blind docking tests of the native Osh4 protein surface for all model ligands, being encountered in 16 top results for PC (-2.88 kcal/mol, most favorable conformation), 19 cases for PIP_2 (-4.86 kcal/mol, most favorable), and all 20 cases for PIP_3 (-5.30 kcal/mol, most favorable) and PS (-5.22 kcal/mol, most favorable). Though nearly all of the lowest energy PIP_2 and PIP_3 conformations docked within this region, several receptor conformations taken from MD snapshots failed to dock PIP_2 or PIP_3 in this region favorably. For these snapshots, PIP_2 and PIP_3 favored the α_4-α_6 region. However, because ΔG^{bind} was typically unfavorable for the α_4-α_6 region in most cases, the region is lowly populated in the top results for PIP_2 (1 result out of 20) and unpopulated for PIP_3. The RMSD analysis presented in Section 2.3.2 demonstrates that the β-barrel, which partially defines the β-crease region, does not structurally deviate significantly with respect to the protein's crystal structure.

An additional RMSD analysis on the second section partially defining the β-crease region, the 393-416 loop, also yielded no significant deviations from the protein's crystal structure (RMSD < 1 Å). Therefore, it is conjectured that specific side chain orientation is responsible for the favorability of some receptor conformations over others to the β-crease site. Though all receptor conformations docked PS well, PS docked to different sites within the β-crease region in a manner largely dependent on receptor conformation. Most results in this region were centered about K168 and/or K180 (Figure

2.13A) though two results were found closer to the 236-244 loop, stabilized by electrostatic interactions between K218 and E232.

Most results in this region were centered about K168 and/or K180 (Figure 2.13A) though two results were found closer to the 236-244 loop, stabilized by electrostatic interactions between K218 and E232.

Residues in the β-crease region found to interact with PC, PS, and both PIP models during these docking studies are situated near several residues identified in Schulz et al.[39] that may interact with liposomes (Figure 2.10B). K168 and K411 were frequently found to interact with all models used during docking tests, while E412C and A169C were two mutations that showed a high degree of cross-linking. The β-crease region was also located near S174, a residue implicated in cysteine-replacement

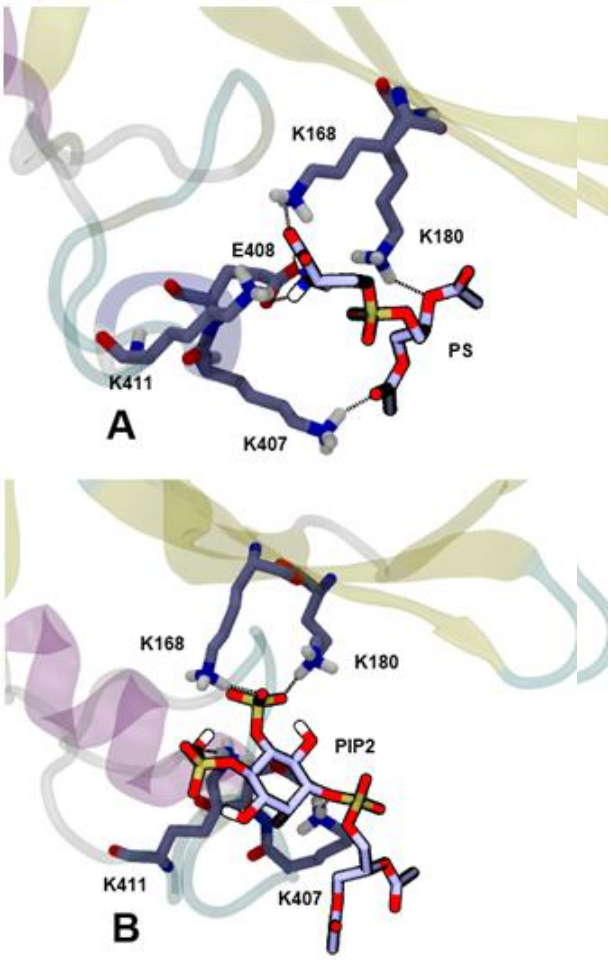

Figure 2.13 - Sample binding conformations of PS and PIP_2 model ligands. **A,** Sample conformation produced through rigid-receptor docking of a PS model ligand is shown with PS highlighted. Osh4 residues interacting with the docked ligand are displayed and labeled. **B,** Snapshot taken from 500-ps MD of PIP_2 with Osh4 interacting residues displayed and PIP_2 highlighted. All hydrogen bonds are shown as dotted lines. Nonpolar hydrogens were simulated in the MD simulation, but are not shown.

studies. Docking results were generally encountered in close proximity with the Osh4 'front' membrane interaction surface (as defined in Schulz et al.[39]) though no models used in these tests docked near the proposed distal binding surface to any significant degree, with the two cases where PC bound to the α_4-α_6 region being the only exceptions (Figure 2.11B). It is important to note that PC binding energetics were heavily influenced by vdW contributions, suggesting that PC was biased towards more 'pocket' like regions of the protein. Therefore, it is unlikely that docking studies using a single PC molecule would be able to detect a large surface on the protein favorable towards interaction with a slab of multiple membrane lipids.

The β-crease region contains a high concentration of basic residues, which were often found to interact with multiple PIP phosphate groups. For PIP ligands, electrostatic interactions tended to dominate over other AD4 force field effects, though, given the creased shape of the pocket, other interaction terms (vdW, desolvation, and hydrogen bonding) were not insignificant. Though PIP_2 conformations tended to interact with multiple lysine residues, only a small proportion of the results displayed conformations where each of the three phosphate groups was complexed with a lysine. Similarly, the maximum observed number of lysine-phosphate groups for PIP_3 was three (Figure 2.12D), and no instances where all PIP_3 phosphates were complexed with lysines was encountered. PIP_2 is believed to be the primary PIP species involved in the stimulation of sterol transport by Osh4 through in vitro experperimentation.[14] Experimentally, it has been shown that a fragment of the Osh4 protein consisting of residues 171-314 is sufficient for PIP_2 as well as inositol-1,4,5-trisphosphate (IP_3) binding.[27] PIP ligands

docked almost exclusively to a region between residues 166-258 while also exhibiting interactions with a nearby region of the protein contained by residues 398-411.

Blind docking using the crystal structure taken from the engineered lidless form of the Osh4 protein as the rigid receptor produced similar results when compared to docking against the full protein structure. PIP ligands favored the β-crease region for all cases selected in the top results for two out of the three receptor conformations obtained from the available crystal structures (PDB codes 1ZI7A and 1ZI7C). The most energetically favorable conformations in this region were -5.11 and -6.38 kcal/mol for PIP_2 and PIP_3, respectively. However, for the third conformation studied (PDB code 1ZI7B), results were exclusively encountered in a distinct region closer to the mouth of the sterol binding pocket characterized by electrostatic interactions with K109 and K336

Ligand	Cluster	Interacting Residues	Avg. Energy
PIP_2	β-crease	P145, P146, Q166, K168, A169, S170, K180 K218, Y220, N397, P399, D406, K407, E408, K411	-4.4
	mouth	K109, P110, L111, N112, L177, I324, I332, K336	-4.64
PIP_3	β-crease	P145, P146, I167, K168, A169, S170, T178 K180, F182, L201, K407, E408, K411	-4.12
	mouth	K109, P110, L111, N112, I167, A169, W317, I324, K336	-3.57
PS	β-crease	K168, A169, S170, T178, K180, F182, L201, E216 G217, K218, Y220, S254, K255, N392, A398, L403 P404, K407, E408, K411, L414	-4.85
	mouth	K109, P110, L111, N112, K336	-4.31*
	α_4-α_6	E48, K94, S95, R100, E102, S103, K108 A293, P296, A297, H299	-4.88

Table 2.5 - Osh4 residues found to interact with docked ligands for rigid receptor tests (*apo* conformation). Only conformations found in the top results are shown and factored into the average binding energies. Average energies denoted with an asterisk only contained one conformation in the top results.

as well as vdW interactions with several nonpolar residues sequentially located near K109. The most energetically favorable conformations in this region were -5.30 kcal/mol for PIP_2 and -3.88 kcal/mol for PIP_3. Interacting residues identified in this region, denoted as the mouth region, are shown in Table 2.5 along with β-crease region interacting residues also identified during the 'engineered-lidless' tests. The mouth region is not solvent accessible when the Osh4 lid remains intact.

The β-crease region was also commonly encountered in PS docking tests (-6.27 kcal/mol, most favorable). PS demonstrated an ability to bind to the mouth region (-4.31 kcal/mol, most favorable), a region near the entrance of the sterol binding tunnel, for one receptor conformation (PDB code 1ZI7B). PS models also docked to the α_4-α_6 region encountered during PC/PIP_2 tests against the native Osh4 protein. However, specific residues identified in the α_4-α_6 region during the lidless tests tend to lie closer to the α_4 helix and away from the α_6 helix due to conformational differences between the *apo* and native Osh4 structures. This area is denoted as the α_4 region (Table 2.5). The PC ligand typically docked near the mouth of the binding tunnel, though most PC docked conformations tended to penetrate deeper into the binding pocket. PC docking in this region may be caused by the ligand's preference towards the sterol binding pocket, an issue that was also encountered during blind docking tests against Osh4 in its native state caused by the absence of the bound sterol in receptor conformations. Due to the high occurrence of PC docking inside of the sterol binding pocket, PC results are not presented in Table 2.5.

The β-crease region was further investigated by allowing for select flexible side chains (K168, K180, K407 and K411). These residues were commonly found to interact

with PIP_2 during blind docking tests. Surprisingly, although K168 was a common interacting residue identified in rigid tests, only a few docked conformations were identified in the top results that showed interaction with this residue. A range of ΔG^{bind} from -10.7 to -9.21 kcal/mol was encountered in the top results for these tests. K180 was found to be the dominant interacting residue, stabilizing the bound conformation through electrostatic interactions with a PIP_2 phosphate and was typically coordinated electrostatically with nearby K407 and/or K411. It should be noted that the calculated ΔG^{bind} was found to be significantly lower when using flexible residues on the protein. This is, in part, caused by an improvement of the protein's intramolecular energetics when transitioning from the unbound to the bound state that is not present when the receptor is completely rigid.

The stability of the binding conformations observed in this region was tested through a brief MD simulation. PIP_2 did not unbind during 500-ps MD simulations of two select representative binding conformations in this region. However, specific lysine-phosphate interactions displayed in the initial coordinates taken from the docked conformation were not always conserved. A sample conformation where PIP_2 is interacting with three lysine residues is displayed in Figure 2.13B. Since backbone conformational changes upon binding are minimal during the timescales of these simulations, it is impossible to produce an exact schematic of the final PIP bound conformation.

PIP_2 docking with flexible protein side chains was also conducted on a sample space restricted to the 236-244 surface loop. Two representative conformations from the folded and extended conformations were analyzed with all side chains located within the

loop chosen to be freely rotatable. The top results from both conformations docked PIP_2 with similar affinities (ΔG^{bind} of -8.63 to -6.55 kcal/mol for the folded conformation and -7.16 to -5.22 kcal/mol for the extended conformation) though neither conformation was able to dock PIP_2 as well as the β-crease region. However, energetic differences between docking to this site and the β-crease region were typically small (1-2 kcal/mol). A wide variety of binding conformations existed for both the folded and extended states of the loop (Figure 2.14). A composite of the interacting residues identified within each region across all docking tests is shown in Figure 2.15.

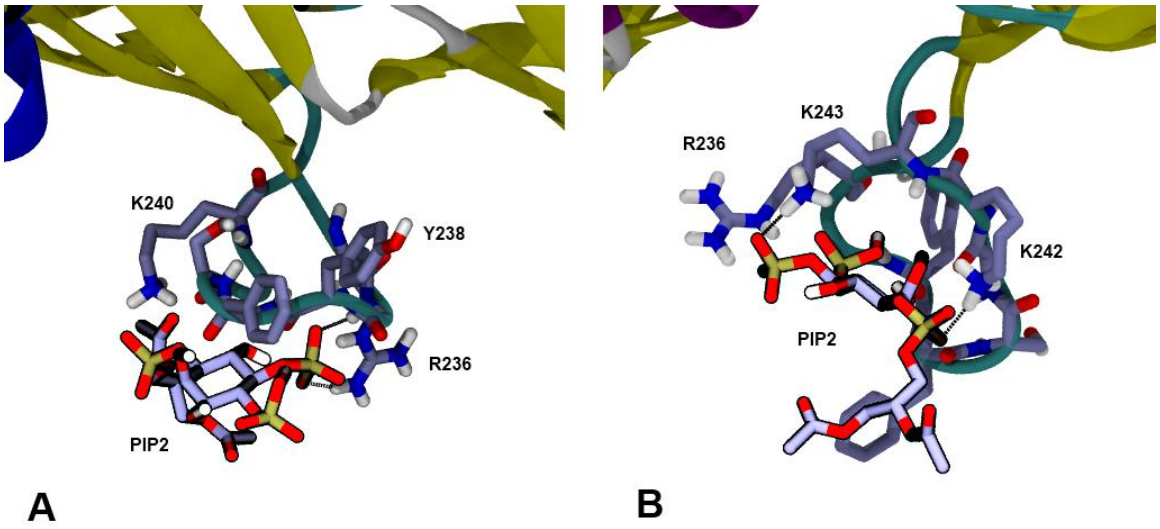

Figure 2.14 - Sample binding conformations of PIP_2 to the 236-244 loop region with flexible side chains. **A,** A sample binding conformation produced through flexible side chain docking to the loop in its folded state. Hydrogen bonds between PIP_2 and Y238/R236 are shown. **B,** A sample binding conformation produced through flexible side chain docking to the loop in its extended state. Hydrogen bonds between PIP_2 and K242/K243 are shown. PIP_2 is highlighted, and only nearby protein residues are displayed.

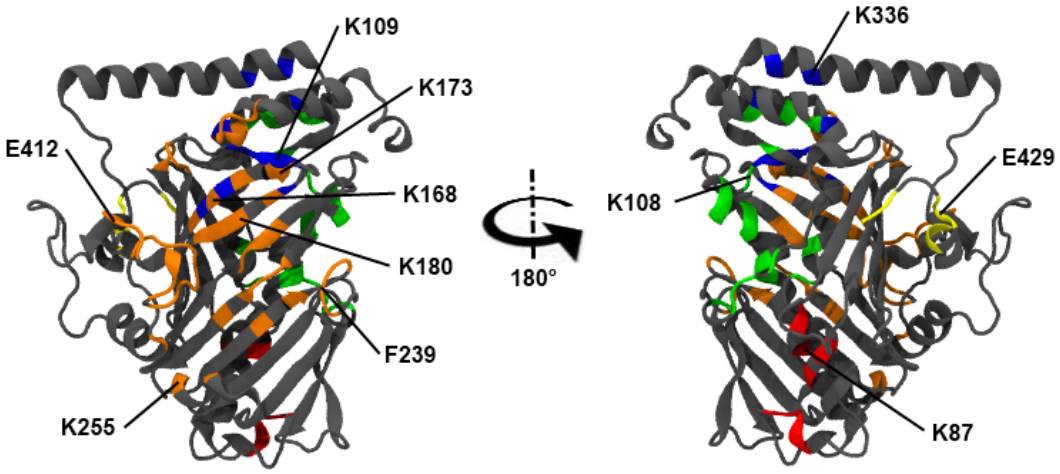

Figure 2.15 - Lipid binding sites encountered on the Osh4 protein. The β-crease region and mouth region (left) are shown in orange and blue, respectively. The opposite side of the protein (right) is shown with the α_3 region in red, the C-terminus region in yellow, and the α_4-α_6 region shown in green. Regions are composed of residues encountered over all docking tests.

CHAPTER 3 – A MODEL YEAST MEMBRANE

3.1 Introduction

Lipids are a diverse group of small hydrophobic or amphiphilic molecules that, generally, fulfill three basic biological functions. Firstly, some lipids such as steryl esters can be used as an efficient means of energy storage within the cell.[41] Secondly, given the propensity for amphiphilic lipids to self associate in water, polar lipids form the basis of cellular membranes through the formation of, most notably, lipid bilayers.[41] Thirdly, many lipids, such as PIP lipids, can act as signaling molecules for interaction with and recruitment of proteins.[41; 42] The variations amongst lipid chains and lipid headgroups allows for a striking diversity in lipid types available within the cell. Moreover, different lipids are not homogeneously distributed across different organelles within the cell.[41] In yeast, several dominant lipid types (divided by headgroup) exist. While a large majority of yeast membranes are comprised of PC, PS, PI, phosphatidylethanolamine (PE), and phosphatidic acid (PA) lipids, several other components such as cardiolipin and various glycolipids exist in small molecular concentrations.[46]

Up until recently, atomistic simulation of biological membranes typically consisted of only one or two types of phospholipids representing the dominant species of the membrane, along with some concentration of a sterol, typically cholesterol.[5; 47] The introduction of the CHARMM-GUI Membrane Builder[48; 49] provides an intuitive graphical user interface that allows for the web-based construction of membrane bilayers with support for over 32 lipid types and cholesterol. This aided in the first MD simulation of a multicomponent membrane designed to represent a true yeast membrane.[49] This

study analyzed several key membrane properties, such as electron-density profiles and surface areas per lipid, of four model yeast membranes. Each membrane consisted of varying and distinct concentrations of six different lipid types using the CHARMM C27r[50; 51] force field.

Previously, the CHARMM C27[52; 53] and the revised C27r force fields were used as the CHARMM parameter set to model membrane phospholipids. However, this force field possessed two notable flaws.[54] The C27/C27r force fields produced a large positive surface tension that, consequentially, reduced the simulated surface area per lipid values to values below experimental estimates when simulated under zero surface tension to represent a flaccid bylayer. This causes a change in the phase of the membrane producing a near gel-like structure, even above the proper gel transition temperature. Secondly, experimental deuterium order parameters (S_{CD}), which measures the order or disorder of C-H bond, demonstrate a splitting for the C_2 carbon of the acyl chain (Figure 2.10 and Appendix) on many glycerophospholipids.[55] This phenomena was not reproducible in MD simulation using the C27 and C27r force field.[54; 56] The newly released CHARMM36 (C36) force field,[54] which contains several updates to the nonbonded and torsional parameters of lipid head group atoms, has been designed to obtain the correct surface area per lipid values when running in tensionless ensembles as well as provide for greatly improved modeling of S_{CD} when compared to previous force fields.

The study presented within this section is concerned with testing the physical properties of a model yeast membrane through MD simulation. Unlike the model membrane systems presented in Jo et al.,[49] this system contains ergosterol, the biological sterol that is present in yeast. Additionally, this simulation will utilize the newly

published C36 force field. Membrane properties such as the surface area per lipid, electron-density profile, aliphatic chain-ordering, and ergosterol tilt angle are analyzed.

3.2 MD Simulation of a Model Yeast Membrane with Ergosterol

3.2.1 Methods

An MD simulation of a model yeast membrane was conducted based off of the equilibrated coordinates of the CPRΔ1 model yeast membrane presented in Jo et al.[49] This membrane was initially modeled after the average lipid content within the membranes of the CPR-Δ1 strain of yeast, though phosphatidylinositol (PI) lipids were not considered as suitable CHARMM force-field parameters were not available. As the CPRΔ1 model contains cholesterol, select coordinates from all cholesterol molecules within the lipid were deleted and rebuilt as the biologically relevant ergosterol residues using an internal coordinate table generated from MD simulation of ergosterol in water. The experimentally determined phospholipid head group concentrations and fatty acid compositions from Daum et al.[57] are presented in Table 3.1, along with the membrane composition of the CPRΔ1-ergosterol membrane used in this simulation. As the initial

	Phospholipid Headgroup						**Unsat. /Sat. ratio**
	PA	PS	PC	PE	PI	Other	
Experimental Composition Percentage (Daum et al.)	6.7	3.3	47.8	20.4	16.2	5.6	7.8
Simulation Composition Percentage	9.5	4.8	57.1	28.6	0	0	9.5

Table 3.1 – Phospholipid composition of yeast membranes. The percentages of each head group are shown, as well as the ratio of unsaturated (unsat.) to saturated (sat.) fatty acid chains.

membrane structure has already been equilibrated, all non-ergosterol residues were fully constrained while ergosterol residues were subject to 1,000 steps of SD minimization followed by 2,000 steps of ABNR minimization in CHARMM.

The system was then equilibrated in NAMD for 500 ps using a 2-fs integrator time step. NAMD version 2.6 does not have the ability to mimic forced-based switching present in CHARMM. This produces a slightly higher attraction between residues and leads to a slight (1-2 $Å^2$) decrease in surface areas per lipid when compared with CHARMM simulations.[55] Pressure was held constant at 1.0 bar using a Langevin piston and the temperature was rescaled every 500 time steps. The surface tension was held at 0.0 dyn/cm^2. After equilibration, 60 ns of constant pressure, surface tension, temperature, and molecular (NPγT) MD simulation was conducted in NAMD. Pressure was held at 1.0 bar using a Langevin piston and Temperature was held at 303.15 K using Langevin dynamics. The surface tension was held at 0.0 dyn/cm^2, which essentially leads to an NPT ensemble. Lennard-Jones interactions were smoothed over the 10-12 Å range and PME[32] was used for long range electrostatics. A tetragonal unit cell was used where the x and y box lengths were constrained to be equivalent. Periodic boundary conditions were used, and hydrogen atoms were constrained using the RATTLE algorithm. After 40 ns of MD simulation, the average surface area per lipid reached a plateau value. Thus, all analysis within this section is completed on the trajectory within the 40-60 ns range. This MD simulation used C36 parameters[55] for all lipids with the exception of ergosterol, which contained parameters and atomic partial charges consistent with all ergosterol simulations within Chapter 2.

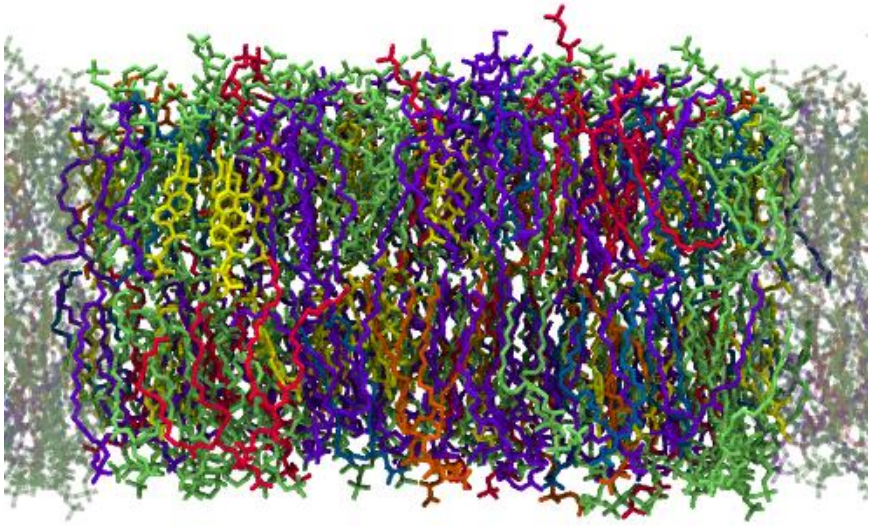

Figure 3.1 – Snapshot of the model yeast membrane. Residues are color coded as follows: DOPC – red; DPPC – orange; POPA – blue; POPE – purple; POPS – red; ergosterol – yellow. Solvent atoms and hydrogens are not displayed here for clarity. Images in the x direction are shown as transparent.

The model yeast membrane system consisted of two leaflets, with each leaflet containing 30 ergosterol residues, 50 DOPC residues, 5 POPS residues, 10 dipalmitoylphosphatidylcholine (DPPC) residues, 10 palmitoyloleoylphosphatidylamine (POPA) residues, and 30 palmitoyloleoylphosphatidylethanolamine (POPE) residues. The system also contained 11,885 TIP3P water molecules, 46 potassium ions, and 16 chlorine ions for a total system size of 67,587 atoms (Figure 3.1). The structures of individual phospholipids can be found in the Appendix section.

3.2.2 Results

In order to ensure that the membrane had reached a proper equilibration, the surface area per lipid was estimated in a manner consistent with Jo et al.[49] by squaring the size of the x-dimension of the crystal and dividing by the total number of lipids per leaflet

(Figure 3.2). After approximately 40 ns, a plateau in the surface area per lipid was reached, and the following 20 ns were used to constitute the production run. During this period, the membrane achieved an average surface area per lipid of 50.3±0.3 $Å^2$, which is slightly lower than the area of 51.6±0.2 $Å^2$ reported for the CPRΔ1 membrane simulations of Jo et al.[49] However, the surface area per lipid for the model yeast membrane was nearly identical to a simulation of the CPRΔ1 membrane using the C36 force field that was conducted by Joseph Lim, a co-author of the Jo et al.[49] paper (50.2 $Å^2$) . The surface areas per individual lipid type were calculated using Voroni tessellation in a manner presented in Pandit et al.[58] and consistent with Jo et al.[48] Three representative atoms on each phospholipid head group were chosen, both carbonyl carbons as well as the carbon where the two acyl chains connect to the phospholipid head group, and projected onto the z=0 plane. One representative atom on each ergosterol residue, the

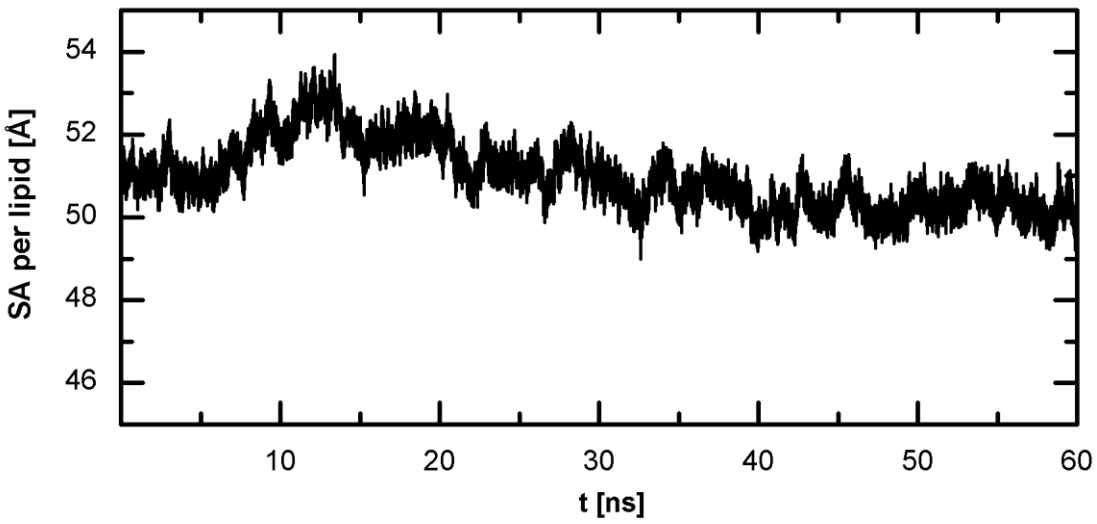

Figure 3.2 – Surface area (SA) per lipid over 60 ns of MD simulation.

	SA [Å^2]					
Model	**Sterol**	**DOPC**	**DPPC**	**POPA**	**POPE**	**POPS**
Yeast-Ergosterol	29.1 ± 0.6	56.9 ± 0.8	57.0 ± 0.9	55.0 ± 1.2	55.7 ± 1.1	55.3 ± 1.5
CPRΔ1 (Jo et al.)	30.7 ± 0.2	58.9 ± 0.3	55.6 ± 0.5	56.4 ± 0.6	57.8 ± 0.4	53.9 ± 1.0
CPRΔ1 - C36	28.7 ± 0.7	57.2 ± 0.7	55.4 ± 1.6	56.3 ± 1.6	55.9 ± 0.8	53.7 ± 2.1

Table 3.2 – Surface area (SA) per lipid by residue type. CPRΔ1 data is taken from Jo et al. CPRΔ1 – C36 data is taken from simulations of the CPRΔ1 membrane using the C36 force field that was conducted by Joseph Lim, a co-author of the Jo et al. paper.

hydroxyl oxygen, was projected onto the z=0 plane. A Delaunay triangulation was constructed for these points, and the circumcenters were calculated and used as the coordinates for the Voroni polygons of the representative atoms used for surface area calculations. These calculations were conducted using the Quickhull program.[59] Calculated surface areas per individual lipid types are presented in Table 3.1. Most lipid types display similar surface areas when compared with Jo et al,.[49] though ergosterol and DOPC show lower surface areas in these simulations. There are no statistically significant differences in residue specific surface area between the ergosterol simulation and a simulation of the CPRΔ1 membrane using the C36 force field that was conducted by Joseph Lim.

Electron density profiles were calculated using the method described in Feller et al.[60] That is, trajectory snapshots were binned into 0.1 Å thick slabs and time averaged to calculate the number of electrons per slab. The total electron density profile is displayed in Figure 3.3A, and shows three distinct regions. The first occurs when |z| is above approximately 30 Å from the center of the bilayer (z = 0 Å), and is represented by a plateau of ~0.34 e Å^{-3}. This region corresponds to the bulk water phase. The second region corresponds to the phospholipid head groups, and is represented as a peak which

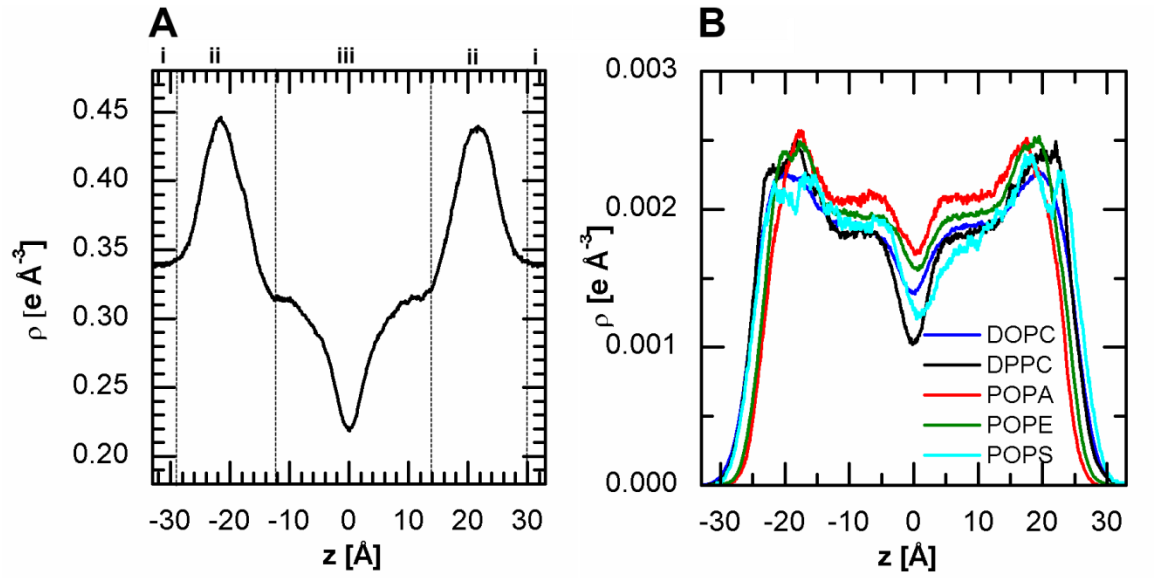

Figure 3.3 – Electron density profiles for the model yeast membrane. **A,** The electron density profile of all system components, including solvent. Regions are marked as follows: i – bulk water phase; ii – phospholipid head groups; iii – low density trough. **B,** Normalized electron density profiles segregated by phospholipid type.

reaches a maximum at |z| ~ 22.6 Å. The third region is a low density trough between the two membrane leaflets at z = 0 Å. The peak-to-peak spacing (X_{HH}) was found to be 45.20 ± 0.2 Å, which is slightly larger than the value reported for the CPRΔ1 membrane (43.0 Å) presented in Jo et al.[49] and also slightly larger than the value reported for the CPRΔ1-C36 membrane simulated by Joseph Lim (43.3 ± 0.2 Å). The normalized electron density profiles for each phospholipid are presented in Figure 3.3B. Unlike the CPRΔ1 membrane from Jo et al.,[49] DOPC did not have the highest density at the center of the bilayer. For this simulation, POPA showed the highest density at the bilayer center, followed by POPE, DOPC, POPS, and DPPC. POPS displayed the largest head group distribution as well as the highest preference for the water phase, as indicated by having the head group distribution the farthest away from the membrane center.

The $|S_{CD}|$ is a measurement of the average angle of the C-H vector with respect to the membrane bilayer normal. A higher $|S_{CD}|$ corresponds to a higher degree of C-H ordering.[49] The $|S_{CD}|$ for each phospholipid type used in this study was calculated using Equation 3.1:

$$|S_{CD}| = \left|\frac{1}{2}\ [3\cos^2(\theta_{CH}) - 1\right| \quad (3.1)$$

The $|S_{CD}|$ order parameters for each individual lipid are shown in Figure 3.4, and the $|S_{CD}|$ of individual hydrogens on each phospholipids C_2 carbon are listed in Table 3.2. Chain splitting on the C_2 carbon is observed for all phospholipids for this simulation, which was not observed in the Jo et al.[49] simulations using the CHARMM C27r force field. While most phospholipids with a monounsaturated bond in one of the side chains displayed statistically indistinguishable, or at least highly similar, $|S_{CD}|$ between the C_9 and C_{10} carbons, a difference between the $|S_{CD}|$ between the C_9 and C_{10} carbons existed. POPS displayed the highest $|S_{CD}|$ of all oleolyl chains beyond the C_9-C_{10} double bond while displaying the lowest $|S_{CD}|$ of all oleolyl chains before this bond.

	Chain 1	
Lipid type	*H2R*	*H2S*
DOPC	0.26 ± 0.002	0.26 ± 0.003
DPPC	0.26 ± 0.01	0.26 ± 0.01
POPA	0.30 ± 0.004	0.26 ± 0.01
POPE	0.27 ± 0.004	0.25 ± 0.004
POPS	0.28 ± 0.01	0.27 ± 0.01
	Chain 2	
Lipid type	*H2R*	*H2S*
DOPC	0.07 ± 0.15	0.01 ± 0.005
DPPC	0.09 ± 0.13	0.01 ± 0.01
POPA	0.10 ± 0.13	0.01 ± 0.01
POPE	0.08 ± 0.01	0.16 ± 0.01
POPS	0.14 ± 0.01	0.16 ± 0.01

Table 3.3 – S_{CD} order parameters for individual hydrogens of the C_2 carbon. For carbon numbering nomenclature, see Appendix.

The orientation of ergosterol with respect to the membrane bilayer normal was calculated by defining a vector over the sterol ring structure through ergosterol's C_3 and C_{17} carbons. The C_3

and C_{17} carbon positions on ergosterol are labeled in Figure 2.7. The probability distribution of ergosterol's tilt angle is shown in Figure 3.5. The mean tilt angle was found to be 18.0° with a most probable angle of 15°. The mean tilt angle reported here is similar to that of the CPRΔ1 membrane from Jo et al. (18.6°).[49] However, the CPRΔ1-C36 simulations conducted by Joseph Lim reveal a mean cholesterol tilt angle of 16.5° with a most probable angle of 12°. Ergosterol was found to posses a 15° tilt of the inertial axis with respect to the diffusional access in ^{13}C-labeled NMR experiments of 16% ergosterol in a DMPC bilayer.[61]

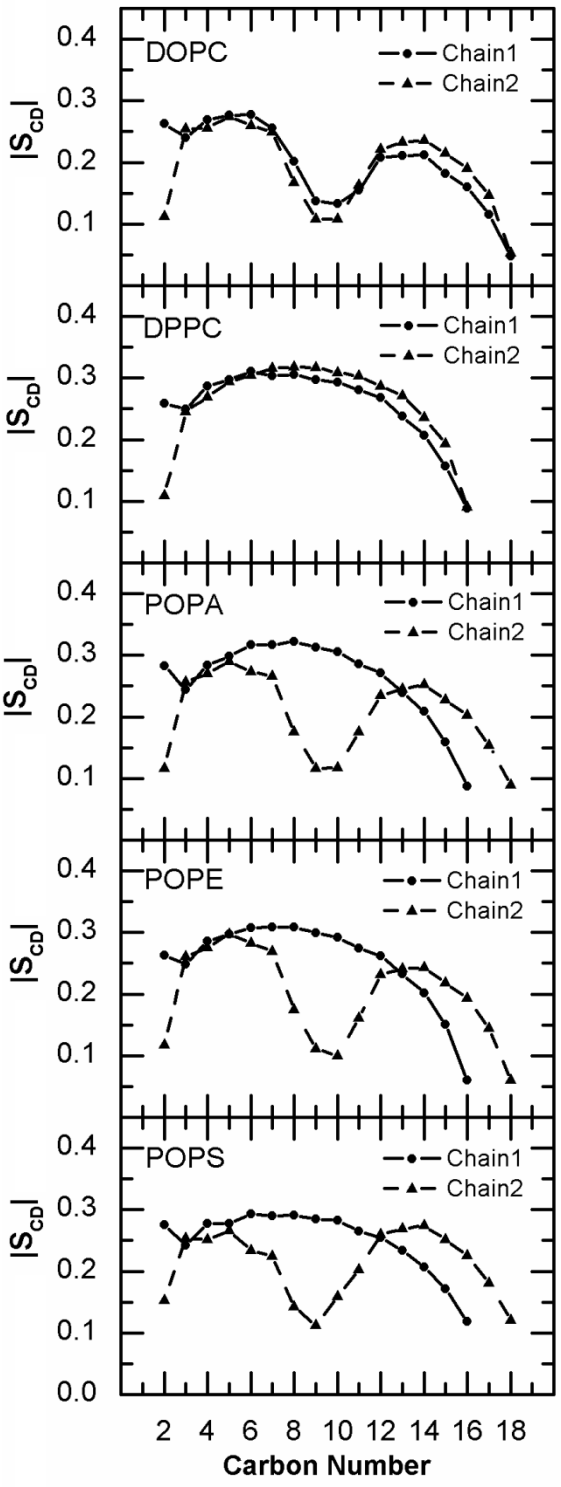

Figure 3.4 – S_{CD} order parameters for all phospholipids. Order parameters for individual hydrogens on the C_2 carbons are shown in Table 3.2.

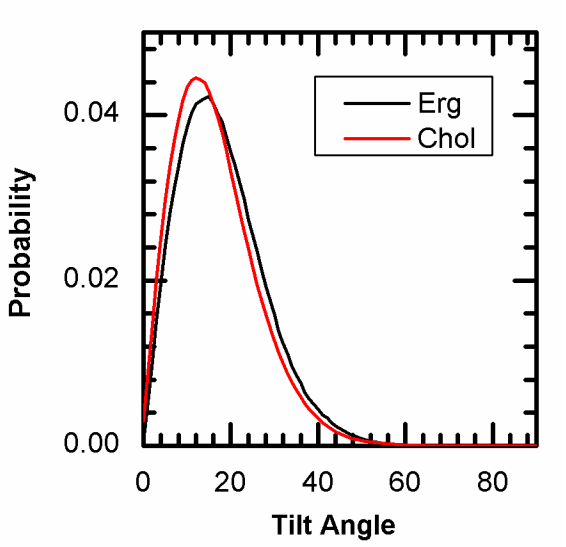

Figure 3.5 – Probability distribution of the tilt angle of ergosterol and cholesterol. Choelsterol data is taken from the CPRΔ1-C36 simulation conducted by Joseph Lim.

CHAPTER 4 – DISCUSSION AND CONCLUSIONS

The discussion of results and conclusions drawn from the simulations presented within this text are presented in two separate sections: one section accounts for Osh4 specific work and the other for membrane specific work. Both the Osh4 and membrane work are inherently important to the ultimate goal of this project, that is, simulating a combined protein and membrane system (see Chapter 5, 'Future Directions'). However, for the purposes of this text, the Osh4 and membrane simulations are separated and treated as separate entities within this section for improved clarity.

4.1 The Osh4 Protein

The sterol binding energetics observed in the Osh4/ergosterol MD simulations were similar to previous MD studies on Osh4/cholesterol conducted in Singh et al.[28] Ergosterol remained tightly bound within the Osh4 binding pocket throughout the course of all simulations, with binding energies dominated by vdW interactions (83%). The F42 side chain, which is located near each sterol's ring structure, is the dominant vdW contributing term (-4.0±0.2 kcal/mol). This residue forms an edge-to-face stacking interaction with ergosterol's ring structure while other nonpolar residues within the binding pocket further stabilize the hydrophobic portion of ergosterol. Similar proline edge-to-face interactions were also seen with P110 (-1.9±0.1 kcal/mol), which is located perpendicular to ergosterol's five membered ring.

Though there was some minor interaction between F13 and ergosterol's tail (Table 2.3), hydrophobic residues on the helical portion of the protein's lid (W10, L14, I17, and F20) did not contribute to the total binding energy to any significant degree.

Ergosterol was primarily stabilized through vdW interactions with hydrophobic residues near the top of the binding pocket (L24, I33, L177, I206, and P211) as well as three nearby charged residues (E107, K108, K109). These simulations do not support the suggestion that hydrophobic residues on the lid directly stabilize the sterol within the binding pocket to any notable degree. However, these residues may stabilize the bound sterol indirectly by occluding the hydrophobic portion of the sterol from unfavorable solvent interaction. Of the three charged residues displaying the most favorable sterol interaction, only E107 posses a side chain that faces towards the inside of the binding pocket. These three residues, especially E107, demonstrated the greatest differences between ergosterol versus cholesterol binding. Given that the largest structural differences between cholesterol and ergosterol occur in the tail, these residues may be important in allowing the binding pocket to accommodate a wide range of sterols. Only modest differences in binding affinities between cholesterol and ergosterol have been observed experimentally.[23]

As in Singh et al.,[28] water-mediated interactions between the 3-OH group of ergosterol and polar residues on the bottom the binding pocket (W46, Q96, Y97, N165, and Q181) were more prevalent than direct hydrogen bonding. Only Q96 was able to form direct hydrogen bonds with ergosterol to any significant degree, though water-mediated interactions were still more common than direct hydrogen bonding for this residue. Waters initially present within the sterol binding pocket during the start of each simulation did not leave the bottom of the binding pocket. Occasionally, water molecules from the bulk phase were able to pass through small gaps between the Osh4 lid and the binding pocket. These waters quickly moved towards the bottom of the binding pocket

and became coordinated with waters already present in the pocket and the 3-OH group of ergosterol.

The structure of Osh4 remained stable throughout the course of MD simulation, as indicated by the RMSD of the protein's carbon backbone atoms (2.09±0.26 Å). However, certain regions of the protein were flexible. One of these regions, the N-terminal lid (residues 1-29), has been suggested to form an ALPS motif in a recent bioinformatics search.[24] The 367-381 loop connecting the α_8 and β_{18} sheet also showed a high level of flexibility. This loop exhibited multiple conformations for many of the MD trajectories, many of which appear unrelated, suggesting that this region may possibly be intrinsically disordered. Any functional consequence of this apparent disorder observed in this region is unknown.

The 236-244 loop was also shown to adopt a multitude of conformations, though these conformations tended to exhibit a higher degree of stability than those of the 367-381 loop (Figure 2.4). Two main conformations were found: a folded state that is present in the crystal structure and an extended state characterized by a dramatic shift in both the hydrogen bonding patterns of select backbone atoms as well as the Ramachandran angles of glycine residues within the loop (Figure 2.6). In the extended conformation, F239 extends away from the protein and into the solvent. While this extension would be energetically unfavorable in solvent, it may aid membrane attachment through favorable interactions with the hydrophobic portion of a membrane bilayer. Several known membrane binding domains, such as typical C1, FYVE, PX, and epsin ENTH domains exhibit hydrophobic protrusions that penetrate into the membrane and help stabilize the bound protein-membrane complex.[26] The model PIP_2 ligand was able to dock to the

folded conformation with a slightly higher affinity than the extended, with a difference in ΔG^{bind} of 1-2 kcal/mol between the two conformations. Blind docking tests against the entire Osh4 surface using PIP_2 and PIP_3 model ligands located a potential binding region loop, in a lysine rich crease centered near K180 (β-crease region). Given the high concentration of positively charged residues in this region, it is possible that a PIP binding event in this region may be driven by long-range electrostatic steering.

During brief MD simulations, PIP_2 did not unbind from this region, though shifts in lysine-phosphate interactions indicate that the initial positioning of the PIP_2 residue with respect to the protein was imperfect (Figure 2.13B). It remains unclear how PIP binding to the β-crease region or the proximal 236-244 loop could facilitate sterol uptake and release from a membrane, given that the locations of both regions lie on a side of the protein that does not run parallel to the mouth of the Osh4 binding pocket. It is possible that PIP binding is accompanied by some conformational change that positions the mouth of the sterol binding pocket in close contact with the membrane or a possible pivot mechanism.[39] The 236-244 loop as well as many residues identified in the β-barrel portion of the β-crease region fall within a fragment of the protein, residues 171-314, that posses the ability to bind to PIP_2 and IP_3.[27] Furthermore, the β-crease region contains K168, a residue that is believed to be important in Osh4's ability to transport cholesterol between vesicles.[14]

The β-crease region (Table 2.4 and Figure 2.10) was favorable towards all lipid moieties tested (PC, PS, PIP_2, and PIP_3), suggesting that this region of the protein would interact favorable with a membrane in close contact. Negatively charged head groups (PS, PIP_2, and PIP_3) had a stronger affinity to this region of Osh4. It has been suggested

that two to three membrane binding surfaces exist on the surface of this protein: a front or lid-area binding surface, a distal binding surface, and a possible third surface along the 236-244 loop (Figure 2.10B).[39] The β-crease region either includes or is adjacent to several residues identified in the front binding surface (A169, S174, and E412). However, a few key residues (S8 and N330) contained on the front binding surface are distant from all residues found in the β-crease region. Furthermore, the β-crease region does not fall on the plane formed by the front binding surface over the mouth of the binding pocket, suggesting that the β-crease region is distinct from this surface. As the β-crease region is located in proximity to the 236-244 loop, it is conceivable that if the protein were to bind to a membrane along β-crease region, the 236-244 loop would be in close contact with the membrane as well.

The docking of model lipids to the engineered lidless protein structure demonstrated that all lipid moieties studied were able to dock near the mouth of the binding pocket (mouth and α_4 region). Lipid binding towards the residues implicated in these site agrees with the proposed mechanism for Osh4-mediated sterol transport suggested by Im et al.[23] That is, charged residues on the mouth of the binding pocket bind to the membrane while the protein is in the lid-open state, allowing for a sterol within the membrane to transfer into the Osh4 binding pocket. Several lipid residues identified within the mouth region (K109, L111, and K336) have been found to be important in sterol transfer between liposomes, especially with PIP_2-containing membranes.[14] While multiple regions of phospholipid affinity were encountered along the Osh4 surface, residues of the α_7 helix as well as the distal binding surface were not captured in our docking studies. This is attributed to the lack of flexibility for backbone atoms along the

Osh4 surface available in these docking studies and suggests protein conformational changes are required to bind to the membrane in these experimentally proposed regions. However, many of the regions identified in our docking tests (Table 2.4 and Table 2.5) are either in or near a conformation that can attract a membrane.

Schulz et al.[39] suggested that the Osh4 protein may pivot between closely apposed membranes, such as an ER-PM membrane contact site, based on experiments where Osh4 was covalently bonded to a membrane with varying linker lengths. Our work predicts a membrane binding surface, the β-crease region, that is located between both the proposed front and distal binding surfaces. This agrees well with the Schulz et al.[39] cross-linking results, and would provide for a surface that could facilitate or initiate pivoting between closely apposed membranes.

It may be possible that PIP_2 binding to the 236-244 loop or a nearby region, such as the β-crease region, could trigger a lid opening event and allow the protein to pivot to a position where nearby mouth residues can bind to the membrane. Such a mechanism would agree with the results from Li et al.,[27] in that the 171-314 region would be subject to PIP_2 binding, as well as the results from Schulz et al.,[39] in that the protein would be able to pivot between membranes so as to move sterols between them. However, the mechanism whereby Osh4 is able to transfer sterols between membranes remains unknown.

4.2 The Model Yeast Membrane

The C36 force field was designed as an improvement over the C27/C27r force fields for several physical properties of phospholipid membrane systems, one of which being the surface area per lipid for a given system.[55] The overall surface area per lipid

(50.3±0.3 Å^2) was lower than the CPRΔ1 model membrane from Jo et al.,[49] with one phospholipid (DOPC) displaying a statistically significant lower surface area per lipid in the ergosterol simulations. However, there were no differences in surface areas per lipid between the model ergosterol membrane and the CPRΔ1-C36 model simulated by Joseph Lim (Table 3.2). Differences between the overall surface area per lipid between CPRΔ1-C36 and CPRΔ1-C27r model systems are caused by the changes to the C36 force field. The condensing effect of ergosterol has been observed to be greater than that of cholesterol in both experimental and computational studies.[5; 62] However, these ordering effects were observed in bilayers that consisted of PC lipids with fully saturated acyl chains, such as DPPC and dimyristoylphosphatidylcholine (DMPC). While DPPC was present in this model system, it only constituted 7.4% of the total membrane lipids and 9.5% of the total membrane phospholipids. The remaining phospholipids contained at least one unsaturated chain.

Ergosterol was found to be inferior to cholesterol in terms of condensing effects in NMR spectroscopy analysis of a 30% sterol, 70% palmitoyloleoylphosphatidylcholine (POPC) bilayer.[62] While all lipids in the model yeast membrane containing one unsaturated side chain (POPA, POPE, and POPS) had similar surface areas when compared against their CPRΔ1-model counterparts, DOPC displayed a lower surface area for the ergosterol simulations. The presence of unsaturated acyl chains within a membrane bilayer is thought to have a complicated relationship with a sterol's ability to condense the bilayer.[62] Currently, no experimental data is available that directly compares the membrane condensing effects of cholesterol and ergosterol on DOPC. However, the data presented here suggests that the relationship between membrane

condensing, sterol structure, and phospholipid chain saturation is complex, and is further complicated by the presence of the non-homogeneity of a membrane with several distinct lipid types.

In the CPRΔ1-C27r force field simulations in Jo et al.,[49] $|S_{CD}|$ values on the chain one C_2 carbon, with the exception of POPS, do not show the proper trend. That is, for these simulations, the $|S_{CD}|$ of the C_2 carbon is lower than the $|S_{CD}|$ of the C_3 carbon where the opposite should be true.[63] This chain splitting on the C_2 carbon is more accurately represented in this ergosterol simulation using the C36 force field (Figure 3.4) when compared with the previous C27 and C27r force fields.[48; 54; 56] Thus, the C36 force field provides a more accurate description of the lipid molecules intramolecular orientation with respect to the bilayer normal for atoms near the glycerol carbon region. As water molecules penetrate into this region of the membrane, properly reproducing the correct conformation in this region should be important with regards to simulating proper water-lipid interactions.

Sterol tilt angles varied between cholesterol and ergosterol (Figure 3.5) across simulations using the C36 force field. Several previous simulation studies have investigated the differences in tilt angles between ergosterol and cholesterol in model membranes with mixed results. Smondyrev and Berkowitz[64] found the average tilt to be higher for ergosterol when compared with cholesterol in a simulation with sterol containing DMPC bilayers using the AMBER forcefield.[22] However, in simulations conducted by Cournia et al.,[5] ergosterol showed a lower tilt angle than cholesterol. These simulations were conducted in CHARMM using the C27 force field and used DPPC bilayers. For the model membrane system studied here, ergosterol contained a tilt of

18.0°, which is higher than the tilt of cholesterol found in the CPRΔ1-C36 simulation conducted by Joseph Lim. Because a smaller sterol tilt is attributed to a stronger ability to order membranes,[65] this data suggests that cholesterol produces a greater ordering affect than ergosterol in this membrane system.

As in Cournia et al.,[5] the thickness of the membrane bilayer, as measured by the electron density profile, was higher in the ergosterol simulation than for the CPRΔ1-C36 simulation by Joseph Lim by 1.9 Å. A slight increase (~1 Å) in membrane thickness of DMPC bilayers with 20% mol ergosterol over bilayers with 20% mol cholesterol was also observed in a small-angle neutron scattering study.[66] One possible explanation for this increase in membrane thickness, as touched on in Pencer et al.,[66] is that the presence of ergosterol has a greater ability to restrict the tilt of the phospholipid acyl chains. As mentioned earlier, the increased tilt angle of ergosterol over cholesterol implies that cholesterol is better at ordering this membrane system. With the exception of the sn-1 chain of DOPC where ergosterol was found to produce increased ordering over the entire chain, S_{CD} parameters on the oleoyl phospholipid chains generally displayed increased ordering with cholesterol in the region between the head group and the C_9-C_{10} double bond while ergosterol displayed increased ordering below this region (based on z-test with $\alpha \leq 0.05$). Palmatoyl chains generally showed better ordering with cholesterol, though differences were commonly statistically insignificant at the $\alpha=0.05$ level below the first few carbons. It would normally be expected that the reduced ordering with ergosterol would also produce a thinner membrane. However, disruption of the tilt of the individual phospholipids by ergosterol would account for the increase in bilayer thickness seen in this simulation as well as experimentally.[66]

CHAPTER 5 – FUTURE DIRECTIONS

While the docking studies presented here provide insight into where a membrane would bind along the Osh4 surface, they only suggest potential mechanisms for membrane binding and sterol transfer. In order to more completely understand how Osh4 mechanistically attaches to PIP-containing membranes and then uptakes or releases a single ergosterol molecule, MD simulations of a combined protein-membrane system will be employed. These simulations will require organelle specific model yeast membranes to be constructed, in part, through use of the CHARMM-GUI Membrane Builder.[49] Currently, the CHARMM-GUI Membrane Builder does not support PI lipids, which play a key role in facilitating Osh4's ability to bind to transfer sterols between vesicles *in vitro*.[14] This problem can be circumnavigated by constructing a membrane in CHARMM-GUI and mutating specific residues as needed before membrane equilibration.

The model yeast membrane presented here is based on the percentages of phospholipid head groups and fatty acids taken from whole yeast cells.[57] Thus, this model is more representative of an average across all yeast organelles. In order to model Osh4 attachment to different membranes within the cell, two membranes would be needed: one to model the ER and one to model the PM. In yeast, the PM is enriched with negatively charged PS lipids while the ER is enriched with charge-neutral PC lipids.[41; 46] Osh4 will be placed in close contact with each membrane in three orientations that model both the lid binding surface and distal binding surface described in Schulz et al.[39] as well as the intermediate, β-crease region that is described here.

As Osh4 has demonstrated the ability to attach to two membranes simultaneously at membrane contact sites, additional simulations will be performed in a dual membrane system. For these simulations, Osh4 will be placed in between a model ER monolayer and a model PM monolayer. Two simulations will be performed, one with the front binding surface in contact with the ER and the distal surface in contact with the PM and another simulation where the surfaces are switched. This will provide a better understanding on how Osh4 binds to membranes simultaneously, as well as allow for the investigation of the proposed pivoting mechanism for sterol transfer between closely apposed membranes suggested in Schulz et al.[39] In order to allow for changes in the Osh4 tertiary structure as well as membrane equilibration, longer simulation timescales will be needed than those presented in the simulations here. While all atom MD simulations of systems of this size are limited to ~100 ns, course-grained force fields are able to approach timescales of multiple microseconds.[67] However, with the appropriate computational hardware and allocation, MD simulations of the microsecond time scales are obtainable.

Understanding the mechanism by which the Osh4 protein transports sterols between membranes will provide important insight into how proper intracellular sterol gradients between membrane organelles are maintained. Given the high sequential homology between the Osh proteins in yeast and similar ORP proteins in mammals, investigation of sterol transport pathways in yeast will aid in understanding these pathways in humans.

APPENDIX

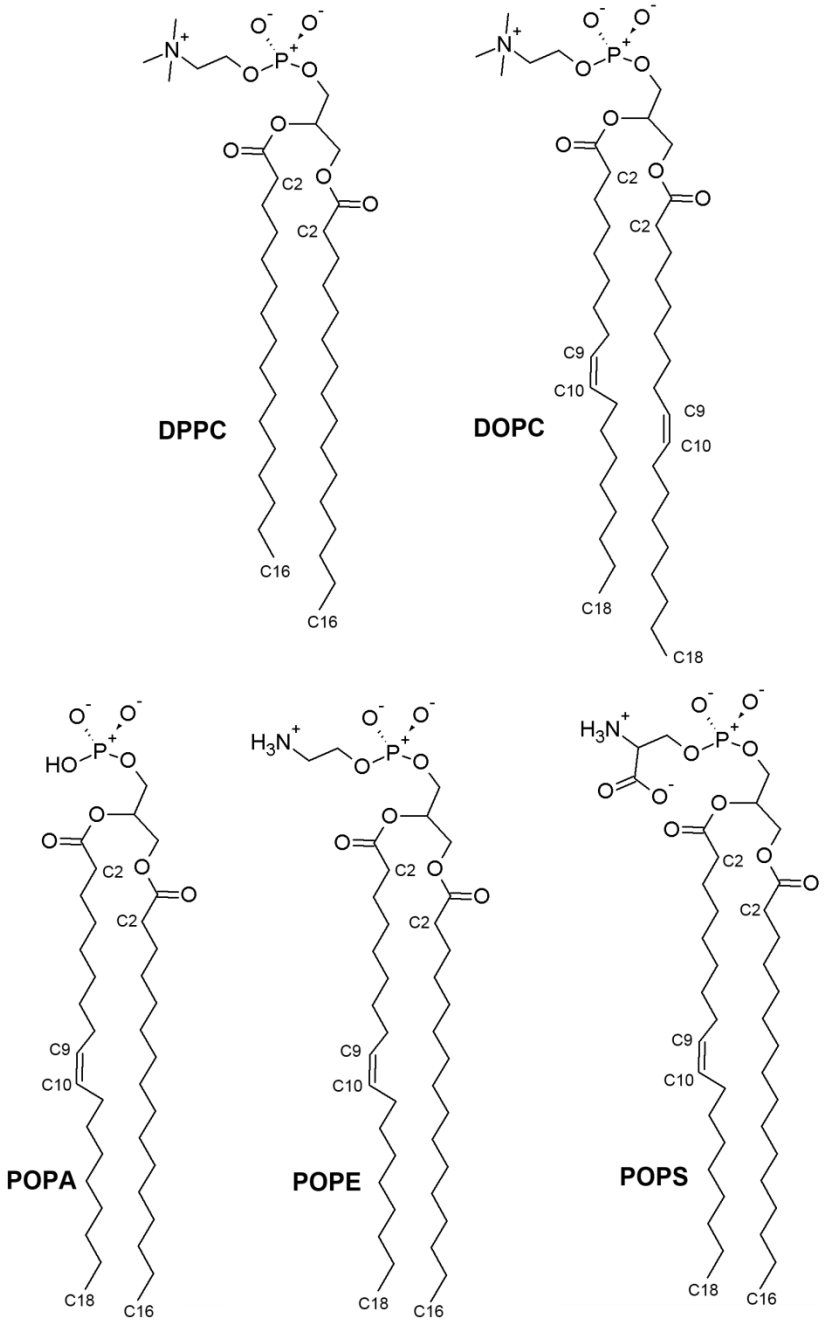

Structures of lipids used in the model yeast membrane simulations. Important carbons are numbered.

REFERENCES

1. Humphrey, W., Dalke, A. & Schulten, K. (1996). VMD: Visual molecular dynamics. *J. Mol. Graphics Modell.* **14**, 33-38.

2. Ikonen, E. (2008). Cellular cholesterol trafficking and compartmentalization. *Nat. Rev. Mol. Cell Biol.* **9**, 125-138.

3. Grundy, S. M. (1983). Absorption and metabolism of dietary cholesterol. *Annu. Rev. Nutr.* **3**, 71-96.

4. Maxfield, F. R. & Menon, A. K. (2006). Intracellular sterol transport and distribution. *Curr. Opin. Cell Biol.* **18**, 379-385.

5. Cournia, Z., Ullmann, G. M. & Smith, J. C. (2007). Differential effects of cholesterol, ergosterol, and lanosterol on a dipalmitoylphosphatidylcholine membrane: a molecular dynamics simulation study. *J. Phys. Chem. B* **111**, 1786-1801.

6. Soccio, R. E. & Breslow, J. L. (2004). Intracellular Cholesterol Transport. *Arterioscler., Thromb., Vasc. Biol.* **24**, 1150-1160.

7. Schulz, T. A. & Prinz, W. A. (2007). Sterol transport in yeast and the oxysterol binding protein homologue (OSH) family. *Biochim. Biophys. Acta* **1771**, 769-780.

8. Simons, K. & Ikonen, E. (2000). How Cells Handle Cholesterol. *Science* **290**, 1721-1726.

9. Silvius, J. R. (2003). Role of cholesterol in lipid raft formation: lessons from lipid model systems. *Biochim. Biophys. Acta* **1610**, 174-183.

10. Hanada, K., Kumagai, K., Yasuda, S., Miura, Y., Kawano, M., Fukasawa, M. & Nishijima, M. (2003). Molecular machinery for non-vesicular trafficking of ceramide. *Nature* **426**, 803-809.

11. Prinz, W. A. (2007). Non-vesicular sterol transport in cells. *Prog. Lipid. Res.* **46**, 297-314.

12. Ngo, M. H., Colbourne, T. R. & Ridgway, N. D. (2010). Functional implications of sterol transport by the oxysterol-binding protein gene family. *Biochem. J.* **429**, 13-24.

13. Beh, C. T., Cool, L., Phillips, J. & Rine, J. (2001). Overlapping functions of the yeast oxysterol-binding protein homologues. *Genetics* **157**, 1117-1140.

14. Raychaudhuri, S., Im, Y. J., Hurley, J. H. & Prinz, W. A. (2006). Nonvesicular sterol movement from plasma membrane to ER requires oxysterol-binding. *J. Cell Biol.* **173**, 107-119.

15. Hansson, T., Oostenbrink, C. & van Gunsteen, W. F. (2002). Molecular dynamics simulations. *Curr. Opin. Struct. Biol.* **12**, 190-196.

16. Leach, A. R. (2001). *Molecular modelling: principles and applications*. 2 edit, Pearson Education Limited.

17. Brooks, B. R., Brooks III, C. L., Mackerell Jr, A. D., Nilsson, L., Petrella, R. J., Roux, B., Won, Y., Archontis, G., Bartels, C., Boresch, S., Caflisch, A., Caves, L., Cui, Q., Dinner, A. R., Feig, M., Fischer, S., Gao, J., Hodoscek, M., Im, W., Kuczera, K., Lazaridis, T., Ma, J., Ovchinnikov, V., Paci, E., Pastor, R. W., Post, C. B., Pu, J. Z., Schaefer, M., Tidor, B., Venable, R. M., Woodcock, H. L., Wu, X., Yang, W., York, D. M. & Karplus, M. (2009). CHARMM: The biomolecular simulation program. *J. Comput. Chem.* **30**, 1545-1614.

18. Hetényi, C. & van der Spoel, D. (2006). Blind docking of drug-sized compounds to proteins with up to a thousand residues. *FEBS Lett.* **580**, 1447-1450.

19. Kirkpatrick, S., Gelatt Jr, C. D. & Vecchi, M. P. (1983). Optimization by simulated annealing. *Science* **220**, 671-680.

20. Morris, G. M., Goodsell, D. S., Halliday, R. S., Huey, R., Hart, W. E., Belew, R. K. & Olson, A. J. (1998). Automated docking using a Lamarckian genetic algorithm and an empiracal binding free energy function. *J. Comput. Chem.* **19**, 1639-1662.

21. Huey, R., Morris, G. M., Olson, A. J. & Goodsell, D. S. (2007). A semiempyrical free energy force field with charge-based desolvation. *J. Comput. Chem.* **28**, 1145-1152.

22. Weiner, S. S., Kollman, P. A., Case, D. A., Singh, U. C., Ghio, C., Alagona, G., Profeta Jr, S. & Weiner, P. (1984). A new force field for molecular mechanical simulation of nucleic acids and proteins. *J. Am. Chem. Soc.* **106**, 765-784.

23. Im, Y. J., Raychaudhuri, S., Prinz, W. A. & Hurley, J. H. (2005). Structural mechanism for sterol sensing and transport by OSBP-related proteins. *Nature* **437**, 154-158.

24. Drin, G., Casella, J.-F., Gautier, R., Boehmer, T., Schwartz, T. U. & Antonny, B. (2007). A general amphipathic α-helical motif for sensing membrane curvature. *Nat. Struct. Mol. Biol.* **14**, 138-146.

25. Lehto, M. & Olkkonen, V. M. (2003). The OSBP-related proteins: a novel protein family involved in vesicle transport, cellular lipid metabolism, and cell signalling. *Biochimica et Biophysica Acta* **1631**, 1-11.

26. Hurley, J. H. (2006). Membrane binding domains. *Biochim. Biophys. Acta* **1761**, 805-811.

27. Li, X., Rivas, M. P., Fang, M., Marchena, J., Mehrotra, B., Chaudhary, A., Feng, L., Prestwich, G. D. & Bankaitis, V. A. (2002). Analysis of oxysterol binding protein homologue Kes1p function in regulation of Sec14p-dependent protein transport from the yeast Golgi complex. *J. Cell Biol.* **157**, 63-77.

28. Singh, R. P., Brooks, B. R. & Klauda, J. B. (2009). Binding and release of cholesterol in the Osh4 protein of yeast. *Proteins: Struct., Funct., Bioinf.* **75**, 468-477.

29. Canagarajah, B. J., Hummer, G., Prinz, W. A. & Hurley, J. H. (2008). Dynamics of cholesterol exchange in the oxysterol binding protein family. *J. Mol. Biol.* **378**, 737-748.

30. Jorgensen, W. L., Chandrasekhar, J., Madura, J. D., Impey, R. W. & Klein, M. L. (1983). Comparison of simple potential functions for simulating liquid water. *J. Chem. Phys.* **79**, 926-935.

31. Hoover, W. G. (1985). Canonical dynamics: Equilibrium phase-space distributions. *Phys. Rev. A* **31**, 1695-1697.

32. Darden, T., York, D. & Pedersen, L. (1993). Particle mesh Ewald: An N log(N) method for Ewald sums in large systems. *J. Chem. Phys.* **98**, 10089-10092.

33. Ryckaert, J.-P., Ciccotti, G. & Berendsen, H. J. C. (1997). Numerical integration of the Cartesian equations of motion of a system with constraints: Molecular dynamics of n-alkanes. *J. Chem. Phys.* **23**, 327-341.

34. Mackerell Jr, A. D., Bashford, D., Bellott, M., Dunbrack Jr, R. L., Evanseck, J. D., Field, M. J., Fischer, S., Gao, J., Guo, H., Ha, S., Joseph-McCarthy, D., Kuchnir, L., Kuczera, K., Lau, F. T. K., Mattos, C., Michnick, S., Ngo, T., Nguyen, D. T., Prodhom, B., Reiher III, W. E., Roux, B., Schlenkrich, M., Smith, J. C., Stote, R., Straub, J., Watanabe, M., Wiorkiewicz-Kuczera, J., Yin, D. & Karplus, M. (1998). All-atom empiracle potential for molecular modeling and dynamics studies of proteins. *J. Phys. Chem. B* **102**, 3586-3616.

35. Pitman, M. C., Suits, F., MacKerell Jr, A. D. & Feller, S. E. (2004). Molecular-level organization of saturated and polyunsaturated fatty acids in a phosphatidylcholine bilayer containing cholesterol. *Biochemistry* **43**, 15318-15328.

36. Phillips, J. C., Braun, R., Wang, W., Gumbart, J., Tajkhorghid, E., Villa, E., Chipot, C., Skeel, R. D., Kale, L. & Schulten, K. (2005). Scalable molecular dynamics with NAMD. *J. Comput. Chem.* **26**, 1781-1802.

37. Mackerell Jr, A. D., Feig, M. & Brooks III, C. L. (2004). Extending the treatment of backbone energetics in protein force fields: Limitations of gas-phase quantum mechanics in reproducing protein conformational distributions in molecular dynamics simulations. *J. Comput. Chem.* **25**, 1400-1415.

38. Andersen, H. C. (1983). RATTLE: A 'velocity' version of the SHAKE algorithm for molecular dynamics calculations. *J. Comput. Phys.* **52**, 24-34.

39. Schulz, T. A., Choi, M.-G., Raychaudhuri, S., Mears, J. A., Ghirlando, R., Hinshaw, J. E. & Prinz, W. A. (2009). Lipid-regulated sterol transfer between closely apposed membranes by oxysterol-binding protein homologues. *J. Cell Biol.* **187**, 889-903.

40. Rogaski, B., Lim, J. B. & Klauda, J. B. (2010). Sterol binding and membrane lipid attachment to the Osh4 protein of yeast. *J. Phys. Chem. B* **114**, 13562-13573.

41. van Meer, G., Voelker, D. R. & Feigenson, G. W. (2008). Membrane lipids: where they are and how they behave. *Nat. Rev. Mol. Cell Biol.* **9**, 112-124.

42. Li, Z., Venable, R. M., Rogers, L. A., Murray, D. & Pastor, R. W. (2009). Molecular dynamics simulations of PIP_2 and PIP_3 in lipid bilayers: Determination of ring orientation, and the effects of surface roughness on a Poisson-Boltzmann description. *Biophys. J.* **97**, 155-163.

43. Gasteiger, J. & Marsili, M. (1980). Iterative partial equalization of orbital electronegativity-a rapid access to atomic charges. *Tetrahedron* **36**, 3219-3288.

44. Morris, G. M., Huey, R., Lindstrom, W., Sanner, M. F., Belew, R. K., Goodsell, D. S. & Olson, A. J. (2009). AutoDock4 and AutoDockTools4: Automated docking with selective receptor flexibility. *J. Comput. Chem.* **30**, 2785-2791.

45. Smart, O. S., Goodfellow, J. M. & Wallace, B. A. (1993). The pore dimensions of gramicidin A. *Biophys. J.* **65**, 2455-2460.

46. Tuller, G., Nemec, T., Hrastnik, C. & Daum, G. (1999). Lipid composition of subcellular membranes of an FY1679-derived haploid yeast wild-type strain grown on different carbon sources. *Yeast* **15**, 1555-1564.

47. Leekumjorn, S. & Sum, A. K. (2006). Molecular simulation study of structural and dynamic properties of mixed DPPC/DPPE bilayers. *Biophys. J.* **90**, 3951-3965.

48. Jo, S., Kim, T., Iyer, V. G. & Im, W. (2008). CHARMM-GUI: A web-based graphical user interface for CHARMM. *J. Comput. Chem.*, 1859-1865.

49. Jo, S., Lim, J. B., Klauda, J. B. & Im, W. (2008). CHARMM-GUI membrane builder for mixed bilayers and its application to yeast membranes. *Biophys. J.* **97**, 50-58.

50. Klauda, J. B., Brooks, B. R., Jr., M. A. D., Venable, R. M. & Pastor, R. W. (2005). An ab initio study on the torsional surface of alkanes and its effect on molecular simulations of alkanes and a DPPC bilayer. *J. Phys. Chem. B* **109**, 5300-5311.

51. Klauda, J. B., Brooks, B. R. & Pastor, R. W. (2005). Adjacent gauche stabilization in linear alkanes: implications for polymer models and conformational analysis. *J. Phys. Chem. B* **109**, 15684-15686.

52. Yin, D. & MacKerell, A. D. J. (1998). Combined ab initio/empyrical approach for optimization of Lennard-Jones parameters. *J. Comput. Chem.* **19**, 334-348.

53. Feller, S. E. & Jr., M. A. D. (2000). An improved empirical potential energy function for molecular simulations of phospholipids. *J. Phys. Chem. B* **104**, 7510-7515.

54. Klauda, J. B., Venable, R. M., Freites, J. A., O'Connor, J. W., Tobias, D. J., Mondragon-Ramirez, C., Vorobyov, I., MacKerell, A. D. J. & Pastor, R. W. (2010). Update of the CHARMM all-atom additive force field for lipids: validation on six lipid types. *J. Phys. Chem. B* **114**, 7830-7843.

55. Klauda, J. B., Venable, R. M., Freites, J. A., O'Connor, J. W., Tobias, D. J., Mondragon-Ramirez, C., Vorobyov, I., MacKerell Jr, A. D. & Pastor, R. W. (2010). Update of the CHARMM all-atom additive force field for lipids: validation on six lipid types. *J. Phys. Chem. B* **114**, 7830-7843.

56. Siu, S. W. I., Vacha, R., Pavel, J. & Bockman, R. A. (2008). Biomolecular simulations of membranes: physical properties from different force fields. *J. Chem. Phys.* **128**, 125103.

57. Daum, G., Tuller, G., Nemec, T., Hrastnik, C., Balliano, G., Cattel, L., Milla, P., Rocco, F., Conzelmann, A., Vionnet, C., Kelley, D. E., Kelley, S., Schweizer, E., Schuller, H.-J., Hojad, U., Greiner, E. & Finger, K. (1999). Systematic analysis of yeast strains with possible defects in lipid metabolism. *Yeast* **15**, 601-614.

58. Pandit, S. A., Vasudevan, S., Chiu, S. W., Mashl, R. J., Jakobsson, E. & Scott, H. L. (2004). Sphingomyelin-cholesterol domains in phospholipid membranes: atomistic simulation. *Biophys. J.* **87**, 1092-1100.

59. Barber, C. B., Dobkin, D. P. & Huhdanpaa, H. (1996). The Quickhull algorithm for convex hulls. *ACM Trans. Math. Softw.* **22**, 469-483.

60. Feller, S. E., Venable, R. M. & Pastor, R. W. (1997). Computer simulation of a DPPC phospholipid bilayer: structural changes as a function of molecular surface area. *Langmuir* **13**, 6555-6561.

61. Soubias, O., Jolibois, F., Massou, S., Milon, A. & Reat, V. (2006). Determination of the orientation and dynamics of ergosterol in model membranes using uniform ^{13}C labeling and dynamically averaged $_{13}$C chemical shift anisotropies as experimental resraints. *Biophys. J.* **89**, 1120-1131.

62. Urbina, J. A., Pekerar, S., Le, H.-b., Patterson, J., Montez, B. & Eric, O. (1995). Molecular order and dynamics of phosphatidylcholine bilayer membranes in the presence of cholesterol, ergosterol and lanosterol: a comparative study using ^{2}H-, ^{13}C- and ^{31}P-NMR spectroscopy. *Biochim. Biophys. Acta* **1238**, 163-176.

63. Schindler, H. & Seelig, J. (1975). Deuterium order parameters in relation to thermodynamic properties of a phospholipid bilayer. A statistical mechanical interpretation. *Biochemistry* **14**, 2283-2287.

64. Smondyrev, A. M. & Berkowitz, M. L. (2001). Molecular dynamics simulation of the structure of dimyristoylphosphatidylcholine bilayers with cholesterol, ergosterol, and lanosterol. *Biophys. J.* **80**, 1649-1658.

65. Aittoniemi, J., Rog, T., Niemela, P., Pasenkiewicz-Gierula, M., Karttunen, M. & Vattulainen, I. (2006). Major factor in sterols' ordering capability in membranes. *J. Phys. Chem. B* **110**, 25562-25564.

66. Pencer, J., Nieh, M.-P., Harroun, T. A., Krueger, S., Adams, C. & Katsaras, J. (2005). Bilayer thickness and thermal response of dimyristoylphosphatidylcholine unilamellar vesicles containing cholesterol, ergosterol and lanosterol: a small-angle neutron scattering study. *Biochim. Biophys. Acta* **1720**, 84-91.

67. Lindahl, E. & Sansom, M. S. (2008). Membrane proteins: molecular dynamics simulations. *Curr. Opin. Struct. Biol.* **18**, 425-431.